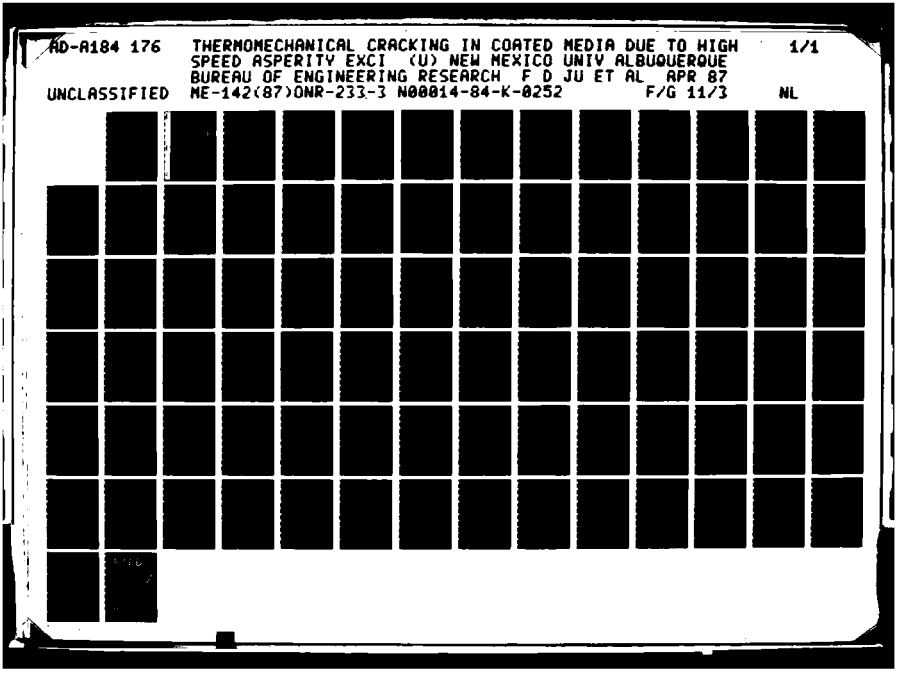
AD-A184 176 THERMOMECHANICAL CRACKING IN COATED MEDIA DUE TO HIGH SPEED ASPERITY EXCI (U) NEW MEXICO UNIV ALBUQUERQUE BUREAU OF ENGINEERING RESEARCH F D JU ET AL APR 87
1/1
UNCLASSIFIED ME-142(87)ONR-233-3 N00014-84-K-0252 F/G 11/3 NL

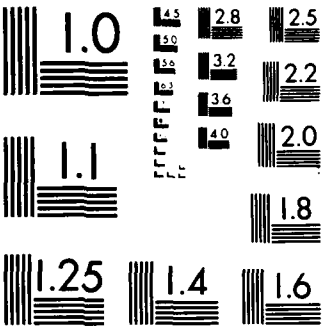

MICROCOPY RESOLUTION TEST CHART
NATIONAL BUREAU OF STANDARDS-1963-A

THE UNIVERSITY OF NEW MEXICO
COLLEGE OF ENGINEERING

BUREAU OF ENGINEERING RESEARCH

Thermomechanical Cracking in Coated Media
Due to High Speed Asperity Excitation

by
Frederick D. Ju and Jew-Chyi Liu
The University of New Mexico

Technical Report
ME-142(87)ONR-233-3

Work performed under ONR Grant No. N00014-84-K-0252

April 1987

Unclassified

SECURITY CLASSIFICATION OF THIS PAGE

REPORT DOCUMENTATION PAGE

1a. REPORT SECURITY CLASSIFICATION: Unclassified	1b. RESTRICTIVE MARKINGS
2a. SECURITY CLASSIFICATION AUTHORITY	3. DISTRIBUTION/AVAILABILITY OF REPORT: Technical Report
2b. DECLASSIFICATION/DOWNGRADING SCHEDULE	
4. PERFORMING ORGANIZATION REPORT NUMBER(S): ME-142(87)ONR-233-3	5. MONITORING ORGANIZATION REPORT NUMBER(S)
6a. NAME OF PERFORMING ORGANIZATION: University of New Mexico; 6b. OFFICE SYMBOL (If applicable)	7a. NAME OF MONITORING ORGANIZATION: Office of Naval Research, Engineering Science Directorate, Material Sci. Div.
6c. ADDRESS (City, State and ZIP Code): Bureau of Engineering Research, University of New Mexico, Albuquerque, NM 87131	7b. ADDRESS (City, State and ZIP Code): 800 N. Quincy Street, Arlington, VA 22217
8a. NAME OF FUNDING/SPONSORING ORGANIZATION: Office of Naval Research; 8b. OFFICE SYMBOL (If applicable): Code (431)	9. PROCUREMENT INSTRUMENT IDENTIFICATION NUMBER
8c. ADDRESS (City, State and ZIP Code): 800 N. Quincy Street, Arlington, VA 22217	10. SOURCE OF FUNDING NOS. — PROGRAM ELEMENT NO. / PROJECT NO. / TASK NO. / WORK UNIT NO.
11. TITLE (Include Security Classification): Thermomechanical Cracking in Coated Media	
12. PERSONAL AUTHOR(S): Frederick D. Ju and Jew-Chy Liu	
13a. TYPE OF REPORT: Technical; 13b. TIME COVERED: FROM 1/86 TO 6/87	14. DATE OF REPORT (Yr., Mo., Day): 87,07,30; 15. PAGE COUNT: 80
16. SUPPLEMENTARY NOTATION	

17. COSATI CODES			18. SUBJECT TERMS (Continue on reverse if necessary and identify by block number)
FIELD	GROUP	SUB. GR.	Asperity; Friction; Coated medium; Coating layer; Substrate; Thermomechanical cracking; Peclet number.

19. ABSTRACT (Continue on reverse if necessary and identify by block number)

This investigation considers the thermo-mechanical effects of an asperity traversing at a high speed over a semi-infinite medium with a thin hard coating surface. The general analytical solutions of the mechanical stress state, the temperature field and the thermal stress state are obtained and expressed in Fourier transform space. The asperity speed is sufficiently high such that the thermal stress is much larger than that caused by the mechanical traction of asperity pressure and friction. The analysis emphasizes the heating effect of mechanical cracking, or "heat-checking" in the surface layer, the substrate or their interface. For hard coating layers, the initiation of a crack will occur at a depth η_{max} (where the maximum principal thermal stresses occur). The depth is found to be controlled principally by the Peclet number. It is found that, for a thick coating layer, the crack will occur inside the surface layer where the stress

(continued on back)

20. DISTRIBUTION/AVAILABILITY OF ABSTRACT: UNCLASSIFIED/UNLIMITED ☒ SAME AS RPT. ☐ DTIC USERS ☐	21. ABSTRACT SECURITY CLASSIFICATION: Unclassified
22a. NAME OF RESPONSIBLE INDIVIDUAL: Dr. A.W. Ruff	22b. TELEPHONE NUMBER (Include Area Code): (202) 696-4401; 22c. OFFICE SYMBOL: ONR COde (431)

DD FORM 1473, 83 APR EDITION OF 1 JAN 73 IS OBSOLETE.

SECURITY CLASSIFICATION OF THIS PAGE

19. Abstract (continued)

state is little affected by the substrate, for which the estimate of fracture initiation is the same as that of a single layer in which the thickness is of the same order of the η_{max}, the interaction between the surface layer and the substrate, through their differences in mechanical and thermal properties, and thus the crack initiation in the neighborhood of η_{max}. The investigation employs the Fourier transform technique for the analytical method in order to facilitate the parametric study. The complex Fourier transform inversion could be done, within the strip of analyticity, along a carefully selected path. The speed of numerical integration can be optimized with the proper choice of the offset, c, from the real axis, which is the theoretical path of integration for Fourier inverse transform.

Technical Report

Thermomechanical Cracking in Coated Media Due to High Speed Asperity Excitation

by

Frederick D. Ju
Presidential Professor

and

Jew-Chyi Liu
Research Assistant

Mechanical Engineering Department
The University of New Mexico
Albuquerque, NM 87131

April 1987

Work performed under ONR Grant No. N00014-84-K-0252

Acknowledgement

The present research is performed under a grant from the Office of Naval Research, Grant No. N00014-84-K-0252. Dr. Peter J. Blau and Dr. A. William Ruff are the program manageers.

Abstract

This investigation considers the thermo-mechanical effects of an asperity traversing at a high speed over a semi-infinite medium with a thin hard coating surface. The general analytical solutions of the mechanical stress state, the temperature field and the thermal stress state are obtained and expressed in Fourier transform space. The asperity speed is sufficiently high such that the thermal stress is much larger than that caused by the mechanical traction of asperity pressure and friction. The analysis emphasizes the heating effect of the friction force, which leads to the initiation of the thermo-mechanical cracking, or "heat-checking" in the surface layer, the substrate or their interface. For hard coating layers, the initiation of a crack will occur at a depth η_{max} (where the maximum principal thermal stresses occur). The depth is found to be controlled principally by the Peclet number. It is found that, for a thick coating layer, the crack will occur inside the surface layer where the stress state is little affected by the substrate, for which the estimate of fracture initiation is the same as that of a single material of the coating. Yet, for modified surfaces of thin coating layer in which the thickness is of the same order of the η_{max}, the interaction between the surface layer and the substrate, through their differences in mechanical and thermal properties, greatly influences the combined stress state near the interface, and thus the crack initiation in the neighborhood of η_{max}. The investigation employs the Fourier transform technique for the analytical method in order to facilitate the parametric study. The complex Fourier transform

inversion could be done, within the strip of analyticity, alor a carefully selected path. The speed of numerical integration can be optimized with the proper choice of the offset, c, from the real axis, which is the theoretical path of integration for Fourier inverse tranform.

Table of Contents

List of Figures

Nomenclature

a	Asperity characteristic dimension, the half width of the contact area
c	Specific heat
C_1, C_1^*	The dilatational wave speed of the surface layer and the substrate, respectively
C_2, C_2^*	The shear wave speed of the surface layer and the substrate, respectively
H	Thickness of the surface layer
k	Thermal conductivity
M	Mach number
$\mathcal{P}(x_1)$	Load distribution over the contact area
P_0	Average pressure over the contact area
$q(x_1)$	Heat flux distribution through the contact area
q_0	Average heat flux through the contact area
R, R_I, R_{II}	Peclet numbers of the single material, surface layer and the substrate, respectively
$\mathcal{R}_i$	Traction over the contact area in the x_i direction
T	Temperature field
u_1, u_2	Displacement in x_1 and x_2 direction, respectively
u, v	Dimensionless displacement in x_1 and x_2 direction, respectively
V	Traverse speed of asperity (x_1 direction)
$\{x_i\}$	Convective coordinates fixed to the moving asperity
$\{x_i'\}$	Material coordinates fixed to the medium
α	Coefficient of thermal expansion
β	The material region: I for the coating surface; II for the substrate
ϕ	Dimensionless temperature field ($=(T-T_0)k/q_0a$)

η_{cr}	Dimensionless depth of maximum principal thermal stress for single material
η_{max}	Dimensionless depth of maximum principal thermal stress for layer medium
κ	Thermal diffusivity
∂_i	Partial derivative with respect to x_i coordinate
$\varepsilon_{11}, \varepsilon_{12}, \varepsilon_{22}$	Strain field
$\{\xi, \eta\}$	Dimensionless coordinates ($-x_i/a$)
λ, μ	Lame's coefficients
μ_f	Coulomb coefficient of friction
$\sigma_{11}, \sigma_{12}, \sigma_{22}$	Stress field
$\sigma_{\xi\xi}, \sigma_{\xi\eta}, \sigma_{\eta\eta}$	Dimensionless stress field
σ_I	Maximum principal thermal stress
ρ	Mass density
δ_{ij}	Kronecker delta
ν	Poisson's ratio

Chapter 1

Introduction and Literature Survey

1.1 Problem of Thermo-mechanical Cracking in Layered Medium

The present investigation studies the asperity and the material parameters which influence the thermo-mechanical cracking in a medium with a surface coating layer. The general failure mechanism is caused by the frictional excitation of a high speed asperity traversing over a coated surface. Maximum tensile stress is considered the principal cause of mode I cracking in the hard wear material. Maximum shearing stress especially in the coating/substrate interface may very well lead to delamination failure of the coating layer. The understanding of such a failure process shall improve the design of these devices by alleviating the problem of friction cracking.

When two bodies in high speed contact under heavy loads slide relative to each other, the nominal design pressure between the mating surfaces is based upon the nominal design contact area. However, at high operating speed, the actual contact area can be reduced by several orders of magnitude. As a result, a low design pressure may result in a very high interfacial pressure in the actual contact zone. Local high temperature may occur due to excessive frictional heating in the vicinity of the contact regions. Cracking may then happen caused by the combined thermal heating and mechanical load leading toward wear and functional failure of the device. This phenomenon is the so-called

"heat checking" or "thermocracking" [1]. Both the reduction . the performance life and the wasted energy are of concern to mechanical designers. For improvement of the wear property of the surface, recent effort has been directed toward surface modification. Research in behavior of coated surface under asperity excitation, hence, has gained importance recently.

A general survey of the problem of cracking through the development of a frictional hot spot was discussed by Burton [2]. A series of experiments carried out by Sibley and Allen [3] showed photographic evidence of symmetrically moving hot patches in the contact zone. Surface displacements and temperature field of a convective elastic half space under an arbitrarily distributed fast-moving line heat source were obtained, using integral transform techniques, by Ling and Mow [4]. The problem of thermal stresses, Mow and Cheng [5], and temperature distribution, Ling and Yang [6], were examined. Two dimensional models of heat checking in the contact zone of a face seal were presented by Ju and Huang [7]. Two dimensional models in the contact zone of a thick layered medium were presented by Ju and Chen [8]. In their two-dimensional analysis of a layered medium, it was shown that the material parameters affect strongly the stress state that would cause thermo-mechanical cracking. The effects of thin coating were shown, but a parametric study of a thinner surface layer was not considered.

1.2 Parametric Effects

The present work deals with a general class of problems for thermo-mechanical cracking that is caused by a moving asperity traversing at a high speed over a semi-infinite medium with a thin surface coated layer. Such a thin surface layer is commonly designed for surface modification to improve the wear property of the substrate, such as a composite, which is generally of poor resistance to friction wear. The frictional excitation of the asperity imparts a mechanical load as well as a thermal load. Through frictional heating onto the surface boundary of the coated layer, the high speed traversing heat source behaves like a thermal shock. It is the combined thermo-mechanical stress state that leads to the initiation of cracks in the surface layer, the substrate or their interface. The stress states depend upon the asperity characteristics, the coating layer thickness, and the material properties of both the coating layer and the substrate. The analysis of the thermo-mechanical field in a layered medium involves the matching of the mechanical and the thermal properties of both the surface layer and the substrate. The asperity characteristics also play an important role. The individual influences can be protracted from works on the parametric analysis of high speed asperity excitation over a single material by Ju and Huang [9,10,11,12], which was a fully three-dimensional model. The parameters, as inferred from the mathematical model, are tabulated as follows;

TABLE I

Asperity Parameters

V	Asperity traversing speed
$\mathcal{P}(x_1)$	Asperity pressure
a	Asperity contact area width

TABLE II

Material Parameters

(λ,μ) or (E,ν)	Mechanical constitutive coefficients
ρ	Mass density
μ_f	Coefficient of Coulomb friction
α	Coefficient of thermal expansion
κ	Thermal diffusivity
k	Thermal conductivity

This paper will expound their effects on the stress states and on the locations of the maximum stress.

1.3 General Theory

At high speed traversing, the high temperature and surface yield due to the excitation are subgranular. The plastic wear and surface shear for hard wear material are demonstrated experimentally to be restricted to a very thin surface layer (Blau [14], and Ruff and Blau [15]). If the critical point of initiation of thermo-mechanical cracking is at a point of depth by an order of magnitude larger than plastic depth, the base solid material subjected to the asperity

friction is essentially elastic. Furthermore, for the present purpose, the material is homogeneous and isotropic without local flaws. The basic mathematical formulas of thermoelasticity describing the behavior of continuous media are the following:

$$\mu\nabla^2\underline{u} + (\lambda+\mu)\text{grad div } \underline{u} = (3\lambda+2\mu)\alpha \text{ grad } T + \rho\ddot{\underline{u}}, \tag{1.1}$$

$$\kappa\nabla^2 T = \rho c\dot{T}, \tag{1.2}$$

where u and T are the displacement and temperature, (λ,μ) are the Lame's elastic coefficients, ρ is the mass density, α is the coefficient of thermal expansion, κ is the thermal diffusivity, and a dot over a variable denotes a time derivative. The justification of the use of the uncoupled form of the Fourier equation is referred to Boley and Wiener [16]. The effect of the dynamic term may result from either a dynamic loading state or a thermal shock in which the rise time of temperature is of the order of time of passage of the stress waves in the material. Duhamel [17] stated that the dynamic term can be disregarded if the time rate of change of temperature is slow enough. Parkus [18] showed that the significant effect from the dynamic term can arise only when there is an instantaneous change in the surface temperature or in the temperature of the surrounding medium. In fact, the dynamic effect is greatly reduced if the temperature change occurs in a very short, but finite, interval of time. This was confirmed by Danilovskaya [19-20], who studied in detail the dynamic effect due to a thermal shock on the surface of a half-space and demonstrated that the maximum dynamic stress is reduced

to 86 percent even for the extremely short duration heating of 10^{-12} seconds. The small effect of the dynamic term, in Equation (1.1), will be neglected and wind up a set of quasi-static uncoupled equations. The quasi-static equations readily allow us to apply the method of integral transforms.

Chapter 2

Problem Statement and Solution Technique

Under consideration is the problem of thermo-mechanical cracking in a coated medium caused by a fast moving asperity whose effect is separated into a moving heat source and a moving mechanical load of combined pressure and tangential friction force. The size of the asperities are of the order of 1 mm; the total thickness of the medium including both the hard wear coating layer and the substrate is at least an order of magnitude larger. Mathematically, the material is represented by a half space with the asperity traversing over the surface boundary at a uniform speed (V) as shown in Figure 1.

2.1 Basic Equations

Two sets of coordinates are considered: x_1'-x_2' are fixed to the medium (the material reference frame), x_1-x_2 are fixed to the moving load (the convective reference frame). The governing differential equations are the thermo-elastic Navier's equation and the uncoupled Fourier equation, respectively, expressed in the material coordinates,

$$(\lambda_\beta+\mu_\beta)\partial_{ij}u_j^\beta + \mu_\beta\partial_{jj}u_j^\beta = \rho_\beta\ddot{u}_j^\beta + (3\lambda_\beta+2\mu_\beta)\alpha_\beta\partial_i T^\beta, \tag{2.1}$$

$$\kappa_\beta\,\partial_{ii}T^\beta = \dot{T}^\beta, \tag{2.2}$$

where $\partial_i = \partial/\partial x_i$, the indices in the subscripts i,j,k have the range

x_1-x_2 are fixed to the moving load

x_1'-x_2' are fixed to the medium

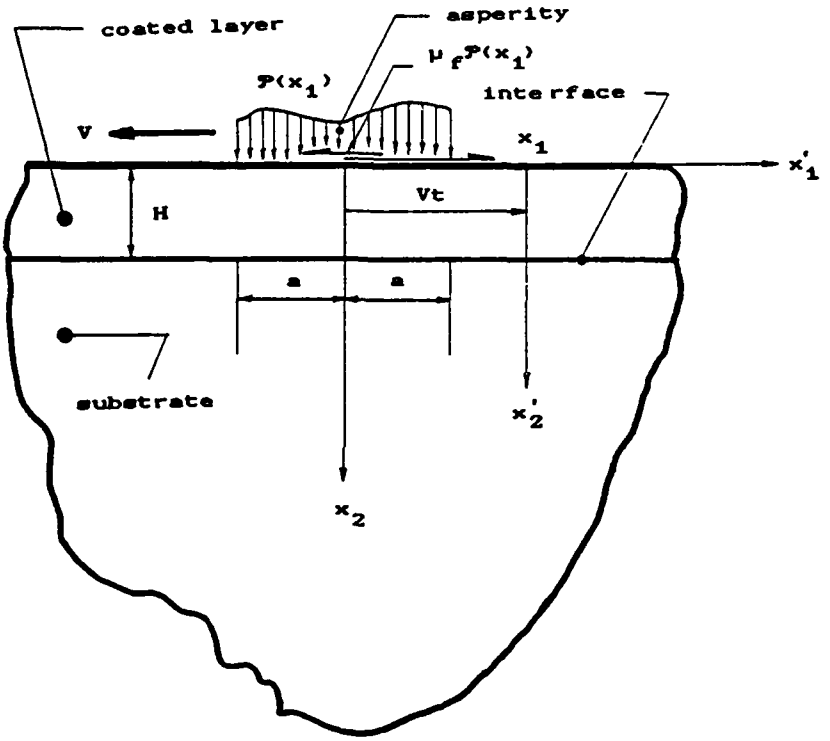

Figure 1. Two Dimension Asperity

1,2; the summation convention is used for all repeated indices of Roman minuscules, β denotes the layered region: I for the coating surface, II for the substrate. The stress field $\{\sigma_{ij}\}$ is related to the displacement field $\{u_i\}$ through the thermo-elastic Hookian law:

$$\sigma_{ij}^{\beta} = \lambda_{\beta}\partial_k u_k^{\beta}\delta_{ij} + \mu_{\beta}(\partial_j u_i^{\beta} + \partial_i u_j^{\beta}) - (3\lambda_{\beta}+2\mu_{\beta})\alpha_{\beta}T^{\beta}\delta_{ij}, \qquad (2.3)$$

where δ_{ij} is the Kronecker delta. The field variables, $\{u_j\}$ and T, as found in Equations (2.1) and (2.2), depend on x_i and t. The configuration shown is Figure 1 changes as time varies. Therefore, time is an explicit variable, and the problem is transient. However, by taking into consideration the uniform properties of the materials, asperity motions and loadings, if the coordinates are fixed to the asperity the configuration remains invariant to time. We thus justify the invariant states of field variables. In other word, with respect to a convective reference frame, the analytical formulation becomes "steady-state"; that is, there is no explicit time variable. The analytical complexity may be alleviated with the use of the convective coordinates $(x_1\text{-}x_2)$. Equations (2.1) and (2.2) become

$$\partial_{ij}u_j^{\beta} + (1-2\nu_{\beta})\partial_{ij}u_i^{\beta} = \mathcal{G}_{\beta}M^2(1-2\nu_{\beta})\partial_{11}u_i^{\beta} + 2(1+\nu_{\beta})\alpha_{\beta}\partial_i T^{\beta}, \qquad (2.4)$$

$$\kappa_{\beta}\partial_{jj}T^{\beta} = V\partial_1 T^{\beta}, \qquad (2.5)$$

where ν_{β} is the Poisson's ratio, $M = [V^2\rho_{II}/\mu_{II}]^{1/2}$ is the Mach number of shear in region II, and $\mathcal{G}_{\beta} = \mu_{II}\rho_{\beta}/\mu_{\beta}\rho_{II}$; i.e. $\mathcal{G}_I = \mu_{II}\rho_I/\mu_I\rho_{II}$, and $\mathcal{G}_{II} = 1$. Time is no longer an explicit variable. The boundary

conditions are:

on the surface, $x_2 = 0$

$$\sigma_{2i}^{I} = -\mathcal{R}_i \tag{2.6}$$

$$k_I \partial_2 T^I = -V\mathcal{R}_2 \tag{2.7}$$

where k_I is the thermal conductivity in the surface layer, $\mathcal{R}_1 = \mu_f \mathcal{P}(x_1)$ and $\mathcal{R}_2 = \mathcal{P}(x_1)$ in the contact region and zero elsewhere. The convective heat loss at the free surface, being of small order, is neglected without loss of generality. Regular conditions hold at infinity; that is, at infinity

$$\sigma_{ij}^{\beta} = 0 \ , \ T^{\beta} = 0 \tag{2.8}$$

The mechanical and the thermal fields must also satisfy the continuity conditions at the layer/substrate interface, $x_2 = H$

$$u_i^I = u_i^{II} \ , \ \sigma_{2j}^{I} = \sigma_{2j}^{II}, \tag{2.9}$$

$$T^I = T^{II} \ , \ k_I \partial_2 T^I = k_{II} \partial_2 T^{II}. \tag{2.10}$$

It is noticed that the governing differential Equation (2.4), and the boundary conditions (2.6) and (2.7), are both non-homogeneous. By separating the fields into two parts, such that

$$\{ \sigma_{ij}^{\beta} \ , \ u_i^{\beta} \} = \{ \sigma_{ij}^{\beta} \ , \ u_i^{\beta} \}_T + \{ \sigma_{ij}^{\beta} \ , \ u_i^{\beta} \}_M, \tag{2.11}$$

where the subscripts T and M represent thermal and mechanical, respectively. The first set shall satisfy the non-homogeneous differential equations with the homogeneous boundary conditions; while the second set shall satisfy the homogeneous differential equations but with the non-homogeneous boundary conditions. Essentially the solutions are delineated into one resulting from the temperature field and another from the mechanical traction. They are, respectively, the thermal stress field and the mechanical stress field. Nevertheless, for single material (equations and solutions see Appendix A), the thermal stress ($\sigma^{T}_{\xi\xi}$) for various speed and mechanical stress ($\sigma^{M}_{\xi\xi}$) are shown, in Figure 2, that if the asperity speed is larger than 0.127 ms^{-1} (5 in/sec), the thermal stress dominates the failure, and the mechanical stress becomes less important. Therefore, for the case of "hot spot", because the asperity traversing speed is much higher (more than 5 ms^{-1}) than the indicated limit speed (0.127 ms^{-1}), the study in the sequel will focus essentially upon the thermal stress.

2.2 Governing Equation

By using the following dimensionless variables:

$$\xi = x_1/a,\ \eta = x_2/a,\ D = H/a,\ u = u_1/a,\ v = u_2/a,$$

$$\sigma_{\xi\xi} = \sigma_{11}/P_0,\ \sigma_{\xi\eta} = \sigma_{21}/P_0,\ \sigma_{\eta\eta} = \sigma_{22}/P_0,$$

$$C_1 = [(\lambda_{II}+2\mu_{II})/\rho_{II}]^{1/2},\ C_2 = (\lambda_{II}/\rho_{II})^{1/2},\ C_1^* = [(\lambda_I+2\mu_I)/\rho_I]^{1/2},$$

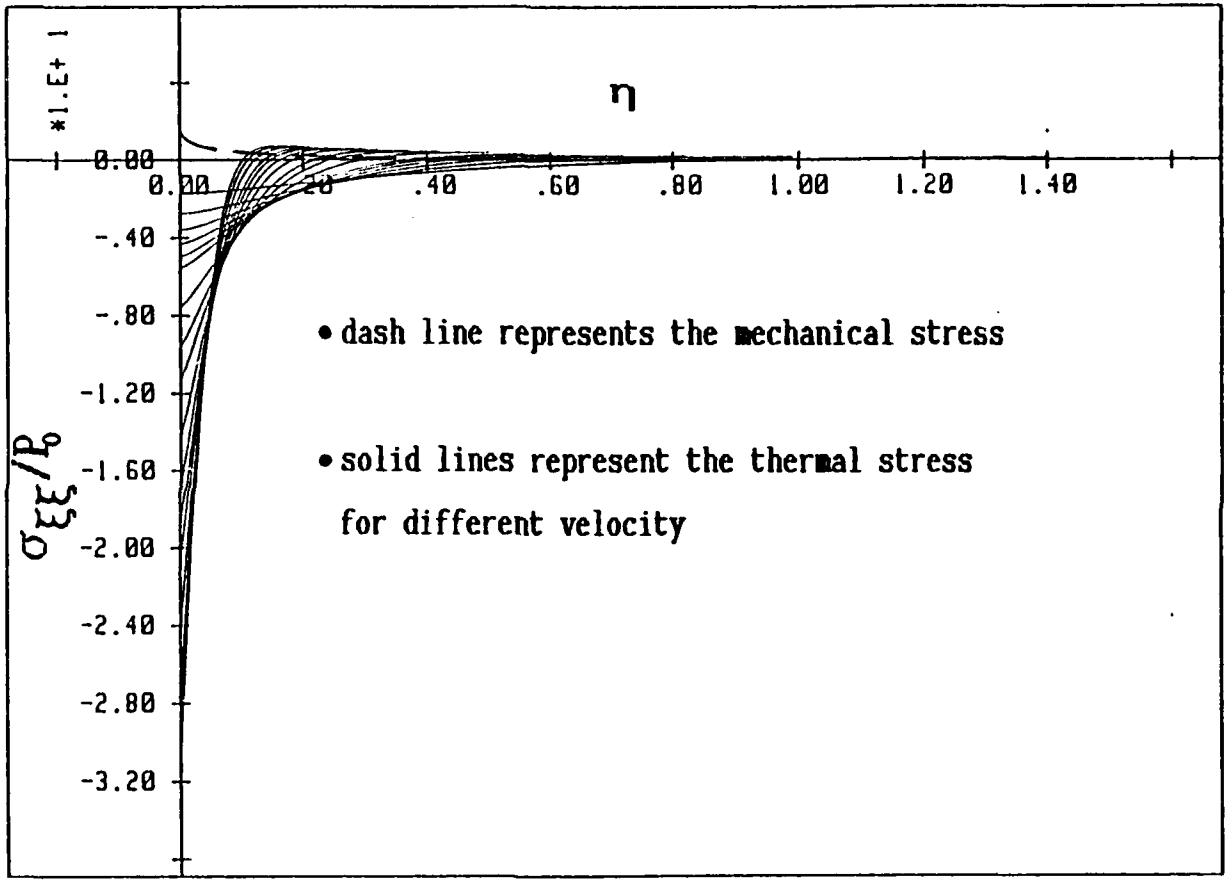

Figure 2. Thermal stress vs. Mechanical stress for different traversing velocities.

$C_2^* = (\lambda_I/\rho_I)^{1/2}$, $b = [(3\lambda_{II}+2\mu_{II})/\rho_{II}]^{1/2}$, $b^* = [(3\lambda_I+2\mu_I)/\rho_I]^{1/2}$,

$\gamma_1 = q_0 a\alpha_I/k_I$, $\gamma_2 = q_0 a\alpha_{II}/k_{II}$, $I = C_1^*/C_2$, $J = C_2^*/C_2$, $\delta = \rho_I/\rho_{II}$,

$M = V/C_2$, $N = C_1/C_2$, $P = \mathcal{P}/P_0$, $Q = q/q_0$, $R_I = Va/\kappa_I$, $R_{II} = Va/\kappa_{II}$,

$\phi^\beta = (T^\beta - T_0)k_I/q_0 a$.

Equation (2.4) becomes:

$$a_\beta \frac{\partial^2 u^\beta}{\partial \xi^2} + (a_\beta - b_\beta)\frac{\partial^2 v^\beta}{\partial \xi \partial \eta} + b_\beta \frac{\partial^2 u^\beta}{\partial \eta^2} - c_\beta \frac{\partial \phi^\beta}{\partial \xi} = \mathcal{S}_\beta M^2 \frac{\partial^2 u^\beta}{\partial \xi^2}, \quad (2.12\text{-a})$$

$$b_\beta \frac{\partial^2 v^\beta}{\partial \xi^2} + (a_\beta - b_\beta)\frac{\partial^2 u^\beta}{\partial \xi \partial \eta} + a_\beta \frac{\partial^2 v^\beta}{\partial \eta^2} - c_\beta \frac{\partial \phi^\beta}{\partial \eta} = \mathcal{S}_\beta M^2 \frac{\partial^2 v^\beta}{\partial \xi^2}, \quad (2.12\text{-b})$$

$$(a_\beta, b_\beta, c_\beta, \mathcal{S}_\beta) = (I^2, J^2, (b^*)^2\gamma_1/C_2^2, 1/J^2), \quad \text{for } \beta = I;$$
$$(a_\beta, b_\beta, c_\beta, \mathcal{S}_\beta) = (N^2, 1, b^2\gamma_1/C_2^2, 1), \quad \text{for } \beta = II,$$

where M is the Mach number in the substrate, and equal to V/C_2, C_2 is the shear wave speed, and V is the traversing speed (or the asperity speed), which is, without loss of generality, of the order of 15 ms^{-1}. $M\mathcal{S}^{1/2}$ denotes, therefore, the Mach number in the surface layer, which for hard wear material, such as Stellite III, is of the order of 10^{-3}. Since the magnitude of $\mathcal{S}M^2$ is of small order to a_β and b_β, the dynamic terms on the right side of equal sign in (2-12-a) and (2-12-b) are negligible comparing to the first terms of both equations

Equation (2-12) thus is simplified to the quasi-static form:

$$a_\beta \frac{\partial^2 u^\beta}{\partial \xi^2} + (a_\beta - b_\beta) \frac{\partial^2 v^\beta}{\partial \xi \partial \eta} + b_\beta \frac{\partial^2 u^\beta}{\partial \eta^2} = c_\beta \frac{\partial \phi^\beta}{\partial \xi}, \qquad (2.13\text{-a})$$

$$b_\beta \frac{\partial^2 v^\beta}{\partial \xi^2} + (a_\beta - b_\beta) \frac{\partial^2 u^\beta}{\partial \xi \partial \eta} + a_\beta \frac{\partial^2 v^\beta}{\partial \eta^2} = c_\beta \frac{\partial \phi^\beta}{\partial \eta}. \qquad (2.13\text{-b})$$

The Hookian law, Equation (2.3), is thus

$$\sigma_{\xi\xi}^{\beta} = \frac{\mu_2}{P_0} d_\beta \left[a_\beta \frac{\partial u^\beta}{\partial \xi} + (a_\beta + b_\beta) \frac{\partial v^\beta}{\partial \eta} - c_\beta \phi^\beta \right], \qquad (2.14\text{-a})$$

$$\sigma_{\xi\eta}^{\beta} = \frac{\mu_2}{P_0} d_\beta b_\beta \left[\frac{\partial v^\beta}{\partial \xi} + \frac{\partial u^\beta}{\partial \eta} \right], \qquad (2.14\text{-b})$$

$$\sigma_{\eta\eta}^{\beta} = \frac{\mu_2}{P_0} d_\beta \left[(a_\beta + b_\beta) \frac{\partial u^\beta}{\partial \xi} + a_\beta \frac{\partial v^\beta}{\partial \eta} - c_\beta \phi^\beta \right]. \qquad (2.14\text{-c})$$

where $d_\beta = \rho_I / \rho_\beta$, that is, $d_I = 1$; $d_{II} = \delta$. The boundary conditions are:

$$\sigma_{\xi\eta}^{I} = \mu_f P(\xi) \quad \text{at } \eta = 0, \quad -1 \le \xi \le 1, \qquad (2.15\text{-a})$$

$$\sigma_{\eta\eta}^{I} = \begin{cases} -P(\xi) & -1 \le \xi \le 1 \qquad \eta = 0 \\ 0 & -1 \ge \xi \text{ and } \xi \ge 1 \quad \eta = 0 \end{cases}, \qquad (2.15\text{-b})$$

$$\sigma_{\xi\xi}^{II},\ \sigma_{\xi\eta}^{II},\ \sigma_{\eta\eta}^{II} \to 0 \quad \text{as} \quad \xi^2 + \eta^2 \to \infty, \qquad (2.16)$$

$$\sigma_{\xi\eta}^{I} = \sigma_{\xi\eta}^{II}, \quad \sigma_{\eta\eta}^{I} = \sigma_{\eta\eta}^{II} \quad \text{at } \eta = D, \qquad (2.17\text{-a})$$

$$v^I = u^{II}, \qquad v^I = v^{II} \qquad \text{at } \eta = D. \qquad (2.17\text{-b})$$

The Fourier equation, Equation (2.5) is expressed in the dimensionless form as:

$$\frac{\partial^2 \phi^\beta}{\partial \xi^2} + \frac{\partial^2 \phi^\beta}{\partial \eta^2} = R_\beta \frac{\partial \phi^\beta}{\partial \xi} \quad . \tag{2.18}$$

In the next section, the solution of these sets of equations, Equations (2.13), (2.14), (2.18) will be obtained, using the Fourier transform method.

2.3 Integral Transform Technique and General Solution

In this section, we will develop in the Fourier transform space the general solutions for the quantities $\{u^\beta, v^\beta, \sigma_{\xi\xi}^\beta, \sigma_{\xi\eta}^\beta, \sigma_{\eta\eta}^\beta\}$.

2.3.1 Fourier Transform

In view of the boundary conditions and the problem itself, by the results in [21], the appropriate representation of the solutions may be obtained by the Fourier transform defined by the following equations:

$$\bar{g}(s,\eta) = \int_{-\infty}^{+\infty} g(\xi,\eta)\exp(is\xi)d\xi \tag{2.19-a}$$

$$g(\xi,\eta) = \frac{1}{2\pi} \int_{-\infty+ic}^{+\infty+ic} \bar{g}(s,\eta)\exp(-is\xi)ds \tag{2.19-b}$$

where s is the complex transform parameter, and $\bar{g}(s,\eta)$ denotes the Fourier transform of $g(\xi,\eta)$. Equation (2.28) forms the Fourier transform pair.

2.3.2 Mechanical Stress Field

With reference to Equations (2.11), (2.13), and (2.14), the equations to be used for the mechanical portion of the solutions are the following:

$$a_\beta \frac{\partial^2 u^\beta}{\partial \xi^2} + (a_\beta - b_\beta)\frac{\partial^2 v^\beta}{\partial \xi \partial \eta} + b_\beta \frac{\partial^2 u^\beta}{\partial \eta^2} = 0, \tag{2.20-a}$$

$$b_\beta \frac{\partial^2 v^\beta}{\partial \xi^2} + (a_\beta - b_\beta)\frac{\partial^2 u^\beta}{\partial \xi \partial \eta} + a_\beta \frac{\partial^2 v^\beta}{\partial \eta^2} = 0, \tag{2.20-b}$$

$$\sigma_{\xi\xi}^{\beta} = \frac{\mu_2}{P_0} d_\beta \left[a_\beta \frac{\partial u^\beta}{\partial \xi} + (a_\beta + b_\beta)\frac{\partial v^\beta}{\partial \eta} \right], \tag{2.20-c}$$

$$\sigma_{\xi\eta}^{\beta} = \frac{\mu_2}{P_0} d_\beta b_\beta \left[\frac{\partial v^\beta}{\partial \xi} + \frac{\partial u^\beta}{\partial \eta} \right], \tag{2.20-d}$$

$$\sigma_{\eta\eta}^{\beta} = \frac{\mu_2}{P_0} d_\beta \left[(a_\beta + b_\beta)\frac{\partial u^\beta}{\partial \xi} + a_\beta \frac{\partial v^\beta}{\partial \eta} \right]; \tag{2.20-e}$$

The boundary conditions, the regularity conditions, and the continuity conditions are, correspondingly,

$$\sigma_{\xi\eta}^{I} = \mu_f P(\xi) \quad \text{at } \eta = 0, \quad -1 \le \xi \le 1, \tag{2.21-a}$$

$$\sigma_{\eta\eta}^{I} = \begin{cases} -P(\xi) & -1 \le \xi \le 1 \qquad \eta = 0 \\ 0 & -1 \ge \xi \text{ and } \xi \ge 1 \quad \eta = 0 \end{cases}, \tag{2.21-b}$$

$$\sigma_{\xi\xi}^{II},\ \sigma_{\xi\eta}^{II},\ \sigma_{\eta\eta}^{II} \to 0 \quad \text{as} \quad \xi^2 + \eta^2 \to \infty, \tag{2.22}$$

$$\sigma_{\xi\eta}^{I} = \sigma_{\xi\eta}^{II}, \qquad \sigma_{\eta\eta}^{I} = \sigma_{\eta\eta}^{II} \quad \text{at } \eta = D, \tag{2.23-a}$$

$$u^I = u^{II}, \qquad v^I = v^{II} \qquad \text{at } \eta = D. \tag{2.23-b}$$

The transformed equations may be obtained by taking the Fourier transform of Equations (2.20-a) through (2.20-e) with respect to ξ:

$$b_\beta \frac{d^2\tilde{u}^\beta}{d\eta^2} - (is)(a_\beta - b_\beta)\frac{dv^\beta}{d\eta} - a_\beta s^2 \tilde{u}^\beta = 0, \qquad (2.24\text{-a})$$

$$a_\beta \frac{d^2\tilde{v}^\beta}{d\eta^2} - (is)(a_\beta - b_\beta)\frac{d\tilde{u}^\beta}{d\eta} - a_\beta s^2 \tilde{v}^\beta = 0, \qquad (2.24\text{-b})$$

$$\tilde{\sigma}_{\xi\xi}^{\beta} = \frac{\mu_2}{P_0} d_\beta \left[(a_\beta - 2b_\beta)\frac{dv^\beta}{d\eta} - (is)a_\beta \tilde{u}^\beta \right], \qquad (2.24\text{-c})$$

$$\tilde{\sigma}_{\xi\eta}^{\beta} = \frac{\mu_2}{P_0} d_\beta b_\beta \left[\frac{d\tilde{u}^\beta}{d\eta} - (is)\tilde{v}^\beta \right], \qquad (2.24\text{-d})$$

$$\tilde{\sigma}_{\eta\eta}^{\beta} = \frac{\mu_2}{P_0} d_\beta \left[a_\beta \frac{d\tilde{v}^\beta}{d\eta} + (a_\beta - 2b_\beta)\tilde{u}^\beta \right]; \qquad (2.24\text{-e})$$

The boundary conditions in the transform space are

$$\tilde{\sigma}_{\xi\eta}^{I} = \mu_f \tilde{P}(s) = \mu_f \int_{-\infty}^{+\infty} P^*(\xi)\exp(is\xi)d\xi \qquad \text{at } \eta = 0, \qquad (2.25\text{-a})$$

$$\tilde{\sigma}_{\eta\eta}^{I} = -\tilde{P}(s) = -\int_{-\infty}^{+\infty} P^*(\xi)\exp(is\xi)d\xi \qquad \text{at } \eta = 0, \qquad (2.25\text{-b})$$

where

$$P^*(\xi) = \begin{cases} -P(\xi) & -1 \le \xi \le 1 \\ 0 & -1 \ge \xi \text{ and } \xi \ge 1 \end{cases}$$

Because the Fourier transform requires the function in the ξ-direction to be either exponentially bounded or to vanish at infinity, therefore, the regularity conditions in the transform space at infinity become:

$$\bar{\sigma}^{II}_{\xi\xi},\ \bar{\sigma}^{II}_{\xi\eta},\ \bar{\sigma}^{II}_{\eta\eta} \rightarrow 0 \text{ as } \quad \eta^2 \rightarrow \infty, \tag{2.26}$$

The boundary conditions become:

$$\bar{\sigma}^{I}_{\xi\eta} = \bar{\sigma}^{II}_{\xi\eta}, \qquad \bar{\sigma}^{I}_{\eta\eta} = \bar{\sigma}^{II}_{\eta\eta} \quad \text{at } \eta = D, \tag{2.27-a}$$

$$\bar{u}^{I} = \bar{u}^{II}, \qquad \bar{v}^{I} = \bar{v}^{II} \quad \text{at } \eta = D. \tag{2.27-b}$$

From Equations (2.24-a) and (2.24-b) we have

$$\bar{u}^{\beta} = -\frac{b_\beta}{a_\beta - b_\beta}\left(\frac{i}{s^3}\right)\frac{d^3\bar{v}^{\beta}}{d\eta^3} - \frac{(a_\beta - 2b_\beta)}{(a_\beta - b_\beta)}\left(\frac{i}{s^3}\right)\frac{d\bar{v}^{\beta}}{d\eta}, \tag{2.28}$$

$$\frac{d^4\bar{v}^{\beta}}{d\eta^4} - 2s^2\frac{d^2\bar{v}^{\beta}}{d\eta^2} + s^4\bar{v}^{\beta} = 0. \tag{2.29}$$

The general solution for Equation (2.29) is

$$\bar{v}^{\beta} = a^*_\beta \exp(-\eta s) + b^*_\beta \exp(\eta s) + c^*_\beta \eta \exp(-\eta s) + d^*_\beta \eta \exp(\eta s). \tag{2.30}$$

Substituting Equation (2.30) into (2.28) we have

$$\bar{u}^{\beta} = i\Big[\, a^*_\beta \exp(-\eta s) - b^*_\beta \exp(\eta s) + \left(\frac{2}{p_\beta} - 1\right)\frac{1}{s}\Big(\, c^*_\beta \exp(-\eta s) +$$

$$+ d^*_\beta \exp(\eta s) + \eta\left(c^*_\beta \eta \exp(-\eta s) - d^*_\beta \eta \exp(\eta s)\right)\Big]\Big], \tag{2.31}$$

where $p_\beta = 1 - a_\beta/b_\beta$. Then, substituting Equation (2.30) and (2.31) into (2.24-c) through (2.24-e), we obtain the mechanical stress field solution for Re[s]>0, as follows:

$$\bar{\sigma}_{\xi\xi}^{\beta} = \frac{\mu_2}{P_0} d_\beta s\Big[2b_\beta\big(a_\beta^* \exp(-\eta s) - b_\beta^* \exp(\eta s)\big) +$$

$$+ 2b_\beta\Big(\frac{2a_\beta - b_\beta}{b_\beta - a_\beta}\Big)\frac{1}{s}\big(c_\beta^* \exp(-\eta s) + d_\beta^* \exp(\eta s)\big) +$$

$$+ 2b_\beta\eta\big(c_\beta^* \exp(-\eta s) - d_\beta^* \exp(\eta s)\big)\Big], \qquad (2.32)$$

$$\bar{\sigma}_{\xi\eta}^{\beta} = \frac{\mu_2}{P_0} (is) d_\beta b_\beta\Big[- 2\big(a_\beta^* \exp(-\eta s) + b_\beta^* \exp(\eta s)\big) -$$

$$- 2\Big(\Big(\frac{1}{p_\beta} - 1\Big)\frac{1}{s} + \eta\Big)c_\beta^* \exp(-\eta s) +$$

$$+ 2\Big(\Big(\frac{1}{p_\beta} - 1\Big)\frac{1}{s} - \eta\Big)d_\beta^* \exp(\eta s)\Big)\Big], \qquad (2.33)$$

$$\bar{\sigma}_{\eta\eta}^{\beta} = \frac{\mu_2}{P_0} d_\beta b_\beta s\Big[-2\big(a_\beta^* \exp(-\eta s) - b_\beta^* \exp(\eta s)\big) -$$

$$- \frac{2}{p_\beta s}\big(c_\beta^* \exp(-\eta s) + d_\beta^* \exp(\eta s)\big) -$$

$$- 2\eta\big(c_\beta^* \exp(-\eta s) - d_\beta^* \exp(\eta s)\big). \qquad (2.34)$$

Using the regularity condition (2.26)

$$b_{II}^* = d_{II}^* = 0. \qquad (2.35)$$

For $\mathrm{Re}[s] < 0$ we can get a similar set of solutions, where a_β^*, b_β^*, c_β^*, and d_β^* are function of s and depend upon the pressure distribution profile $\bar{P}$ given by

$$\bar{P} = \frac{2\sin(s)}{s} , \qquad (2.36)$$

for a uniform unit pressure in the contact region, $-1 \le \xi \le 1$.

Now enforcing the boundary conditions (2.25) and (2.27), the six coefficients a_I^*, b_I^*, c_I^*, d_I^*, a_{II}^*, and c_{II}^* can be solved from six algebraic equations. The six algebraic equations may be presented in matrix form as Equation (2.37), and to be solved in Chapter 3 by Gaussian elimination using the computer subroutine "DECOMP".

Let $\mathcal{A}_\beta = [(2/p_\beta - 1)/s + D]e^{-Ds}$ $\quad \mathcal{B}_I = [(2/p_I - 1)/s - D]e^{-Ds}$

$\mathcal{C}_\beta = [(1-1/p_\beta)/s - D]e^{-Ds}$ $\quad \mathcal{D}_I = [(1-1/p_I)/s + D]e^{-Ds}$

$\mathcal{E}_\beta = -[(1/(p_\beta s) + D]e^{-Ds}$ $\quad \mathcal{F}_I = -[(1/(p_I s) - D]e^{-Ds}$

and

$$\Delta \, \mathcal{U}_M = \mathcal{F}_M \qquad (2.37)$$

where

$$\Delta = \begin{bmatrix} -1 & -1 & (1-1/p_I)/s & -(1-1/p_I)/s & 0 & 0 \\ -1 & 1 & -1/p_I s & -1/p_I s & 0 & 0 \\ e^{-Ds} & -e^{Ds} & \mathcal{A}_I & \mathcal{B}_I & -e^{-Ds} & -\mathcal{A}_{II} \\ e^{-Ds} & e^{Ds} & De^{-Ds} & De^{Ds} & -e^{-Ds} & De^{-Ds} \\ -e^{-Ds} & -e^{Ds} & \mathcal{C}_I & \mathcal{D}_I & e^{-Ds}/\delta J^2 & -\mathcal{C}_{II}/\delta J^2 \\ -e^{-Ds} & e^{Ds} & \mathcal{E}_I & \mathcal{F}_I & e^{-Ds}/\delta J^2 & -\mathcal{E}_{II}/\delta J^2 \end{bmatrix}$$

$$u_M = \begin{Bmatrix} a_I^* \\ b_I^* \\ c_I^* \\ d_I^* \\ a_{II}^* \\ c_{II}^* \end{Bmatrix} \qquad \mathfrak{F}_M = \begin{Bmatrix} \mu_f \bar{P}/\delta J^2 \\ -\bar{P}\delta J^2 \\ 0 \\ 0 \\ 0 \\ 0 \end{Bmatrix}$$

2.3.3 Temperature Field

The governing differential equation for the temperature field, Equation (2.18), is restated here:

$$\frac{\partial^2 \phi^\beta}{\partial \xi^2} + \frac{\partial^2 \phi^\beta}{\partial \eta^2} = R_\beta \frac{\partial \phi^\beta}{\partial \xi}, \qquad \beta = I, II. \tag{2.18}$$

The boundary conditions, the regularity conditions, and the continuity conditions are

$$-\frac{\partial \phi^\beta}{\partial \eta} = Q^*(\xi) = \begin{cases} -Q(\xi) & -1 \le \xi \le 1 \quad \eta = 0 \\ 0 & -1 \ge \xi \text{ and } \xi \ge 1 \quad \eta = 0 \end{cases}, \tag{2.38}$$

$$\frac{\partial \phi^I}{\partial \eta} = \mathcal{B} \frac{\partial \phi^{II}}{\partial \eta}, \qquad \eta = D, \tag{2.39-a}$$

$$\phi^I = \phi^{II}, \qquad \eta = D, \tag{2.39-b}$$

$$\phi^I, \ \phi^{II} \to 0, \qquad \text{as } \xi^2+\eta^2 \to \infty \tag{2.40}$$

where $\mathcal{B} = k_{II}/k_I$. Equation (2.18) in transform space becomes

$$\frac{d^2\tilde{\phi}^\beta}{d\eta^2} - (s^2 - iR_\beta s)\tilde{\phi}^\beta = 0. \tag{2.41}$$

The solution of Equation (2.50) is

$$\tilde{\phi}^\beta = A'_\beta \exp(-\sqrt{s^2 - iR_\beta s}\ \eta) + B'_\beta \exp(\sqrt{s^2 - iR_\beta s}\ \eta), \tag{2.42}$$

where $\mathrm{Re}[\sqrt{s^2 - iR_\beta s}] \geq 0$, A'_β, and B'_β are function of s and depend upon the heat input profile $\tilde{Q}^*$ given by

$$\tilde{Q} = \frac{2\sin(s)}{s}, \tag{2.43}$$

for uniform unit pressure and friction. Using the regularity condition (2.40)

$$B'_{II} = 0. \tag{2.44}$$

Applying the boundary conditions (2.38) and (2.39), the three coefficients A'_I, B'_I and A'_{II} can be readily found:

$$A'_I = \frac{\tilde{Q}^*(F_I + \mathcal{B}F_{II})}{F_I^2\left(1-\exp(-2F_I D)\right) + \mathcal{B}F_I F_{II}\left(1+\exp(-2F_I D)\right)}, \tag{2.45-a}$$

$$B'_I = \frac{\tilde{Q}^*(F_I + \mathcal{B}F_{II})\exp(-2F_I D)}{F_I^2\left(1-\exp(-2F_I D)\right) + \mathcal{B}F_I F_{II}\left(1+\exp(-2F_I D)\right)}, \tag{2.45-b}$$

$$A'_{II} = \frac{2\tilde{Q}^*\exp\left((F_{II} - F_I)D\right)}{F_I^2\left(1-\exp(-2F_I D)\right) + \mathcal{B}F_I F_{II}\left(1+\exp(-2F_I D)\right)}, \tag{2.45-c}$$

where $F_I = \sqrt{s^2 - iR_I s}$, $F_{II} = \sqrt{s^2 - iR_{II} s}$, $\mathrm{Re}[F_{II}] \geq 0$, and $\mathrm{Re}[\quad] \geq 0$.

2.3.4. Thermal Stress Field

From Equations (2.11), (2.13), and (2.14), the equations for the thermal component of the solutions are:

$$a_\beta \frac{\partial^2 u^\beta}{\partial \xi^2} + (a_\beta - b_\beta) \frac{\partial^2 v^\beta}{\partial \xi \partial \eta} + b_\beta \frac{\partial^2 u^\beta}{\partial \eta^2} = c_\beta \frac{\partial \phi^\beta}{\partial \xi}, \tag{2.46-a}$$

$$b_\beta \frac{\partial^2 v^\beta}{\partial \xi^2} + (a_\beta - b_\beta) \frac{\partial^2 u^\beta}{\partial \xi \partial \eta} + a_\beta \frac{\partial^2 v^\beta}{\partial \eta^2} = c_\beta \frac{\partial \phi^\beta}{\partial \eta}, \tag{2.46-b}$$

$$\sigma_{\xi\xi}^\beta = \frac{\mu_2}{P_0} d_\beta \left[a_\beta \frac{\partial u^\beta}{\partial \xi} + (a_\beta + b_\beta) \frac{\partial v^\beta}{\partial \eta} - c_\beta \phi^\beta \right], \tag{2.46-c}$$

$$\sigma_{\xi\eta}^\beta = \frac{\mu_2}{P_0} d_\beta b_\beta \left[\frac{\partial v^\beta}{\partial \xi} + \frac{\partial u^\beta}{\partial \eta} \right], \tag{2.46-d}$$

$$\sigma_{\eta\eta}^\beta = \frac{\mu_2}{P_0} d_\beta \left[(a_\beta + b_\beta) \frac{\partial u^\beta}{\partial \xi} + a_\beta \frac{\partial v^\beta}{\partial \eta} - c_\beta \phi^\beta \right]. \tag{2.46-e}$$

The boundary conditions, the regularity conditions, and the continuity conditions are

$$\sigma_{\xi\eta}^I = 0 \quad \text{at } \eta = 0, \quad -1 \leq \xi \leq 1, \tag{2.47-a}$$

$$\sigma_{\eta\eta}^I = 0 \quad \text{at } \eta = 0, \quad -1 \leq \xi \leq 1, \tag{2.47-b}$$

$$\sigma_{\xi\xi}^{II}, \ \sigma_{\xi\eta}^{II}, \ \sigma_{\eta\eta}^{II} \to 0 \text{ as } \quad \xi^2 + \eta^2 \to \infty, \tag{2.48}$$

$$\sigma_{\xi\eta}^I = \sigma_{\xi\eta}^{II}, \qquad \sigma_{\eta\eta}^I = \sigma_{\eta\eta}^{II} \quad \text{at } \eta = D, \tag{2.49-a}$$

$$u^I = u^{II}, \qquad v^I = v^{II} \qquad \text{at } \eta = D. \tag{2.49-b}$$

Equation (2.46) in the transformed space become:

$$b_\beta \frac{d^2\tilde{u}^\beta}{d\eta^2} - (is)(a_\beta - b_\beta)\frac{dv^\beta}{d\eta} - a_\beta s^2 \tilde{u}^\beta = -(is)c_\beta \tilde{\phi}^\beta, \tag{2.50-a}$$

$$a_\beta \frac{d^2\tilde{v}^\beta}{d\eta^2} - (is)(a_\beta - b_\beta)\frac{d\tilde{u}^\beta}{d\eta} - a_\beta s^2 \tilde{v}^\beta = c_\beta \frac{d\tilde{\phi}^\beta}{d\eta} \tag{2.50-b}$$

$$\tilde{\sigma}_{\xi\xi}^{\ \beta} = \frac{\mu_2}{P_0} d_\beta \left[(a_\beta - 2b_\beta)\frac{dv^\beta}{d\eta} - (is)a_\beta \tilde{u}^\beta - c_\beta \tilde{\phi}^\beta \right], \tag{2.50-c}$$

$$\tilde{\sigma}_{\xi\eta}^{\ \beta} = \frac{\mu_2}{P_0} d_\beta b_\beta \left[\frac{d\tilde{u}^\beta}{d\eta} - (is)\tilde{v}^\beta \right], \tag{2.50-d}$$

$$\tilde{\sigma}_{\eta\eta}^{\ \beta} = \frac{\mu_2}{P_0} d_\beta \left[a_\beta \frac{d\tilde{v}^\beta}{d\eta} + (a_\beta - 2b_\beta)\tilde{u}^\beta - c_\beta \tilde{\phi}^\beta \right]. \tag{2.50-e}$$

The boundary conditions, the regularity conditions, and the continuity conditions are transformed into the expressions (see comments before equation (2.26))

$$\tilde{\sigma}_{\xi\eta}^{\ I} = 0 \qquad \text{at } \eta = 0, \tag{2.51-a}$$

$$\tilde{\sigma}_{\eta\eta}^{\ I} = 0 \qquad \text{at } \eta = 0, \tag{2.51-b}$$

$$\tilde{\sigma}_{\xi\xi}^{II}, \ \tilde{\sigma}_{\xi\eta}^{II}, \ \tilde{\sigma}_{\eta\eta}^{II} \to 0 \qquad \text{as } \eta^2 \to \infty, \tag{2.52}$$

$$\tilde{\sigma}_{\xi\eta}^{\ I} = \tilde{\sigma}_{\xi\eta}^{II}, \qquad \tilde{\sigma}_{\eta\eta}^{\ I} = \tilde{\sigma}_{\eta\eta}^{II} \qquad \text{at } \eta = D, \tag{2.53-a}$$

$$\tilde{u}^I = \tilde{u}^{II}, \qquad \tilde{v}^I = \tilde{v}^{II} \qquad \text{at } \eta = D. \tag{2.53-b}$$

From Equations (2.50-a) and (2.50-b) we have

$$\bar{u}^{\beta} = -\frac{b_{\beta}}{a_{\beta}-b_{\beta}}\left(\frac{i}{s^3}\right)\frac{d^3\bar{v}^{\beta}}{d\eta^3} - \frac{(a_{\beta}-2b_{\beta})}{(a_{\beta}-b_{\beta})}\left(\frac{i}{s^3}\right)\frac{d\bar{v}^{\beta}}{d\eta} +$$

$$+\frac{b_{\beta}c_{\beta}}{a_{\beta}(a_{\beta}-b_{\beta})}\left(\frac{i}{s}\right)\frac{\partial^2\bar{\phi}^{\beta}}{\partial\eta^2} + \frac{c_{\beta}}{a_{\beta}}\left(\frac{i}{s}\right)\bar{\phi}^{\beta}, \qquad (2.54)$$

$$\frac{d^4\bar{v}^{\beta}}{d\eta^4} - 2s^2\frac{d^2\bar{v}^{\beta}}{d\eta^2} + s^4\bar{v}^{\beta} = E_{\beta}\frac{\partial^3\bar{\phi}^{\beta}}{\partial\eta^3} - E_{\beta}s^2\frac{\partial\bar{\phi}^{\beta}}{\partial\eta}, \qquad (2.55)$$

where $E_{\beta} = c_{\beta}/a_{\beta}$. Equation (2.55) is a fourth order nonhomogeneous ordinary differential equation, where the nonhomogeneous part comes from temperature field. The complementary $c\bar{v}^{\beta}$ solution of Equation (2.55) is

$$c\bar{v}^{\beta} = A^{*}_{\beta}\exp(-\eta s) + B^{*}_{\beta}\exp(\eta s) + C^{*}_{\beta}\eta\exp(-\eta s) + D^{*}_{\beta}\eta\exp(\eta s). \qquad (2.56)$$

Let the particular solution $p\bar{v}^{\beta}$ of Equation (2.55) be given by

$$p\bar{v}^{\beta} = \Psi_{\beta}\exp(-F_{\beta}s) + \Omega_{\beta}\exp(F_{\beta}s). \qquad (2.57)$$

Substituting Equation (2.57) into (2.55), we obtain:

$$\Psi_{\beta} = \frac{-F_{\beta}E_{\beta}}{F^2_{\beta}-s^2}A'_{\beta}, \qquad \Omega = \frac{F_{\beta}E_{\beta}}{F^2_{\beta}-s^2}B'_{\beta}. \qquad (2.58)$$

The general solution of Equation (2.55) is obtained by combining the complementary and the particular solutions. That is:

$$\tilde{v}^{\beta} = A_{\beta}^{*} \exp(-\eta s) + B_{\beta}^{*} \exp(\eta s) + C_{\beta}^{*}\eta \exp(-\eta s) + D_{\beta}^{*}\eta \exp(\eta s -$$

$$+ \Psi_{\beta} \exp(-F_{\beta}s) + \Omega_{\beta} \exp(F_{\beta}s). \qquad (2.59)$$

Substituting Equation (2.59) into (2.54) we have

$$\tilde{u}^{\beta} = i\Big[A_{\beta}^{*} \exp(-\eta s) - B_{\beta}^{*} \exp(\eta s) + (\frac{2}{p_{\beta}} - 1)\frac{1}{s}\Big(C_{\beta}^{*} \exp(-\eta s) +$$

$$+ D_{\beta}^{*} \exp(\eta s) + \eta\big(C_{\beta}^{*}\eta \exp(-\eta s) - D_{\beta}^{*}\eta \exp(\eta s)\big) -$$

$$- G_{\beta} \exp(-F_{\beta}s) - H_{\beta} \exp(F_{\beta}s)\Big], \qquad (2.60)$$

where

$$G_{\beta} = \Big[\frac{1}{p_{\beta}} (\frac{F_{\beta}}{s})^{3} - (\frac{1}{p_{\beta}} + 1)(\frac{F_{\beta}}{s})\Big] \Psi_{\beta} + E_{\beta}\Big[\frac{1}{p_{\beta}} (\frac{F_{\beta}}{s})^{2} - 1\Big] \frac{A_{\beta}'}{s},$$

$$H_{\beta} = \Big[\frac{1}{p_{\beta}} (\frac{F_{\beta}}{s})^{3} + (\frac{1}{p_{\beta}} + 1)(\frac{F_{\beta}}{s})\Big] \Omega_{\beta} + E_{\beta}\Big[\frac{1}{p_{\beta}} (\frac{F_{\beta}}{s})^{2} - 1\Big] \frac{B_{\beta}'}{s}.$$

Equations (2.59) and (2.60) together with(51-c),(51-d), and (51-e) yield

$$\tilde{\sigma}_{\xi\xi}^{\beta} = \frac{\mu_2}{p_o} d_{\beta} s\Big[2b_{\beta}\big(a_{\beta}^{*} \exp(-\eta s) - b_{\beta}^{*} \exp(\eta s)\big) +$$

$$+ 2b_{\beta}\Big(\frac{2a_{\beta} - b_{\beta}}{b_{\beta} - a_{\beta}}\Big)\frac{1}{s}\Big(c_{\beta}^{*} \exp(-\eta s) + d_{\beta}^{*} \exp(\eta s)\Big) +$$

$$+ 2b_{\beta}\eta\big(c_{\beta}^{*} \exp(-\eta s) - d_{\beta}^{*} \exp(\eta s)\big) +$$

$$+ K_{\beta} \exp(-F_{\beta}s) - L_{\beta} \exp(F_{\beta}s)\Big], \qquad (2.61)$$

$$\tilde{\sigma}^{\beta}_{\xi\eta} = \frac{\mu_2}{P_0}\,(is)d_\beta b_\beta\Big[- 2\big(a^*_\beta \exp(-\eta s) + b^*_\beta \exp(\eta s)\big) -$$

$$- 2\Big(\big(\frac{1}{p_\beta} - 1\big)\frac{1}{s} + \eta\Big)c^*_\beta \exp(-\eta s) +$$

$$+ 2\Big(\big(\frac{1}{p_\beta} - 1\big)\frac{1}{s} - \eta\Big)d^*_\beta \exp(\eta s)\Big) -$$

$$- N_\beta \exp(-F_\beta s) - M_\beta \exp(F_\beta s)\Big], \qquad (2.62)$$

$$\tilde{\sigma}^{\beta}_{\eta\eta} = \frac{\mu_2}{P_0}\, d_\beta b_\beta s\Big[-2\big(a^*_\beta \exp(-\eta s) - b^*_\beta \exp(\eta s)\big) -$$

$$- \frac{2}{p_\beta s}\big(c^*_\beta \exp(-\eta s) + d^*_\beta \exp(\eta s)\big) -$$

$$- 2\eta\big(c^*_\beta \exp(-\eta s) - d^*_\beta \exp(\eta s)\big) +$$

$$+ \frac{Q_\beta}{b_\beta} \exp(-F_\beta s) - \frac{W_\beta}{b_\beta} \exp(F_\beta s)\Big], \qquad (2.63)$$

where

$$K_\beta = -a_\beta G_\beta - (a_\beta - 2b_\beta)\big(\frac{F_\beta}{s}\big)\Psi_\beta - \big(\frac{C_\beta}{s}\big)A'_\beta,$$

$$L_\beta = -a_\beta H_\beta - (a_\beta - 2b_\beta)\big(\frac{F_\beta}{s}\big)\Omega_\beta - \big(\frac{C_\beta}{s}\big)B'_\beta,$$

$$N_\beta = G_\beta\big(\frac{F_\beta}{s}\big) + \Psi_\beta,$$

$$M_\beta = H_\beta\big(\frac{F_\beta}{s}\big) + \Omega_\beta,$$

$$Q_\beta = -(a_\beta - 2b_\beta)G_\beta - a_\beta\big(\frac{F_\beta}{s}\big)\Psi_\beta - \big(\frac{C_\beta}{s}\big)A'_\beta,$$

$$W_\beta = -(a_\beta - 2b_\beta)H_\beta - a_\beta\left(\frac{F_\beta}{s}\right)\Omega_\beta - \left(\frac{C_\beta}{s}\right)B'_\beta.$$

Using the regularity condition (2.61)

$$b^*_{II} = d^*_{II} = 0. \tag{2.64}$$

Applying the boundary conditions (2.51) and continuity conditions (2.53), the six coefficients A^*_I, B^*_I, C^*_I, D^*_I, A^*_{II}, and C^*_{II} can be solved from six algebraic equations. They have been represented in matrix form as equation (2.65), to be solved in Chapter 3 by Gaussian elimination using the computer subroutine "DECOMP".

$$\Delta\, \mathbf{u}_T = \mathfrak{F}_T \tag{2.65}$$

where

$$\text{Transport matrix of } \mathbf{u}_T = \left\{ A^*_I \quad B^*_I \quad C^*_I \quad D^*_I \quad A^*_{II} \quad C^*_{II} \right\}$$

and

$$\mathfrak{F}_T = \left\{ \begin{array}{c} (N_I+M_I)/2 \\ -(Q_I+W_I)/2J^2 \\ -G_{II}\exp\left(-F_{II}D\right) + G_I\exp\left(-F_ID\right) + H_I\exp\left(F_ID\right) \\ \Psi_{II}\exp\left(-F_{II}D\right) + \Psi_I\exp\left(-F_ID\right) + \Omega_I\exp\left(F_ID\right) \\ \left\{-N_{II}\exp\left(-F_{II}D\right)/\delta J^2 + N_I\exp\left(-F_ID\right) + M_I\exp\left(F_ID\right)\right\}/2 \\ \left\{Q_{II}\exp\left(-F_{II}D\right)/\delta J^2 - G_I\exp\left(-F_ID\right)/J^2 - W_I\exp\left(F_ID\right)/J^2\right\}/2 \end{array} \right\}$$

Chapter 3

Numerical Solution

3.1 Selection of Branch Cuts

In discussing a correspondence $w = h(z)$ we use the word "function" to mean that h assigns a single value w to each permissible value of z. Sometimes this fact is emphasized by saying " h is a single-valued function". Of course there are equations which do not define single-valued functions. For example, in the solution of temperature field (2.51), $F_\beta = \sqrt{s^2 - \imath R_\beta s}$ is not a single-valued function in the complex s-plane. Indeed, for each nonzero s, there are two distinct values of F_β. Since the concept of analyticity was defined only for single-valued functions, we can not directly discuss this property for multiple-valued fucntions such as $F_\beta = \sqrt{s^2 - \imath R_\beta s}$. We shall, however, investigate the analyticity of certain single-valued functions which can be derived from a multiple-valued function $w = h(z)$. We construct these single-valued functions by focusing our attention on a domain D and selecting a single-value function which is analytic in D, and then we call it a BRANCH of $h(z)$ in D.

To define the branch of the double-valued function on $F_\beta = \sqrt{s^2 - \imath R_\beta s}$ such that $\mathrm{Re}[F_\beta] \geq 0$, we write

$$F_\beta = (s^2 - \imath R_\beta s)^{1/2} = s^{1/2} \, (s - \imath R_\beta s)^{1/2}, \tag{3.1}$$

and carefully define, using Figure 3, $s^{1/2} = \ell_1 \exp(\imath \theta_1)$, $(s - \imath R_\beta)^{1/2} =$

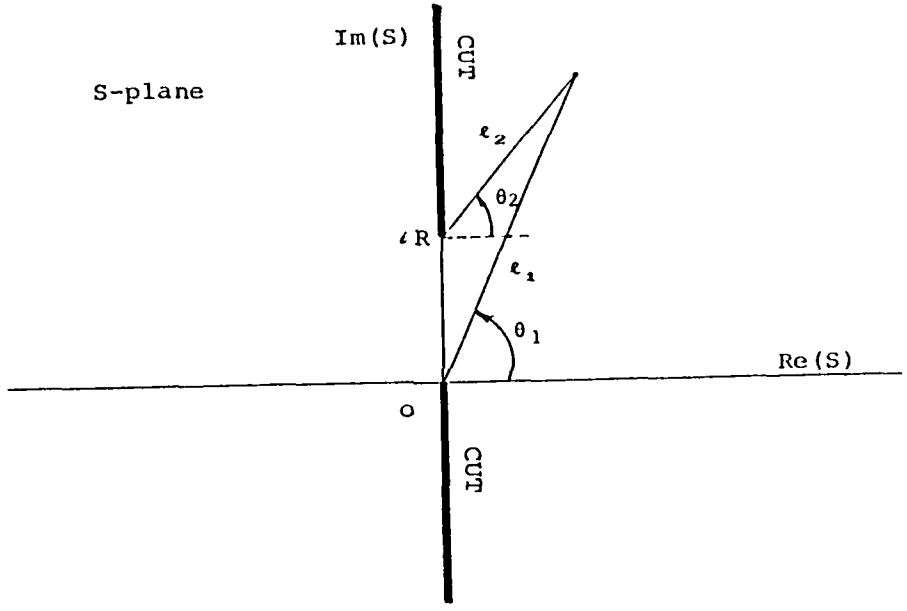

Figure 3. Branch cut selection.

$\ell_2 \exp(i\theta_2)$, with the values for θ_1 and θ_2 shown below. One can select the branch cuts along the imaginary axis in the s-plane, and the range of θ_1, θ_2 such that

$$-\pi/2 \le \theta_1 < 3\pi/2 \tag{3.2-a}$$

and

$$-3\pi/2 \le \theta_2 < \pi/2 \tag{3.2-b}$$

so

$$F_\beta = (\ell_1 \cdot \ell_2)^{1/2} \exp\left[i(\theta_1+\theta_2)/2\right] \tag{3.3}$$

Note: 1. For the points along the real axis and along the imaginary axis between $(0,R_\beta)$, $-\pi/4 < \arg(F_\beta) \le 0$.

2. For the points just left to the cut $(0,-\infty)$, or left to the cut (R_β,∞), $\arg(F_\beta) = \pi/2$.

3. For the points just left to the cut $(0,-\infty)$, or left to the cut (R_β,∞), $\arg(F_\beta) = -\pi/2$.

3.2 Outline of the Computer Program

In simple applications of Fourier transforms, the transform parameter s is a real variable and the path of inverse Fourier transform coincides with the real axis. In view of the expression in Equations (2.42), (2.61), (2.62), and (2.63), there are branch point at the origin an at $s = iR_\beta$. There is also a pole at the origin. The integral is therefore singular. According to the branch cut selection, we can have a strip of analyticity as shown in Figure 4. Knowing from complex analysis [21] that, if the function $\tilde{g}(s,\eta)$ is analytic in a

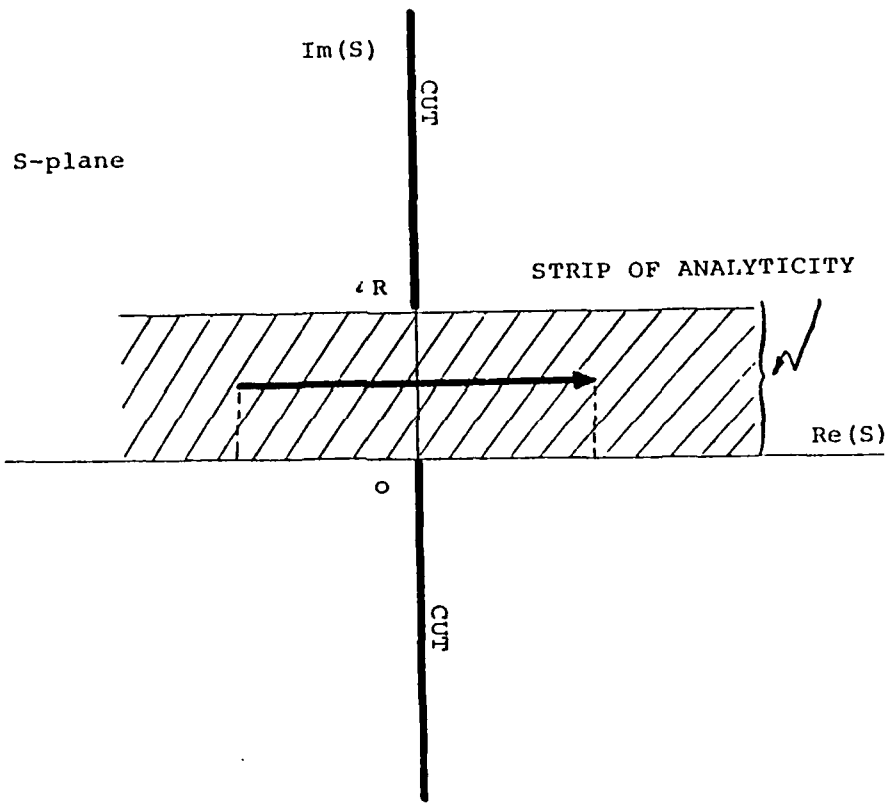

Figure 4. Strip of Analyticity.

domain D, the integral is independent of the path. Therefore within this strip of analyticity, we can translate the integral path parallel to the real axis over a distance c to avoid the singularities.

All solutions, obtained in Chapter 2, are in the transform space. Physical solutions are obtained with inverse transforms. In general, the general solutions, Equations (2.30,31,32,33,34,42,59,60,61,62,63), are too difficult to invert analytically. Numerical inversion is possible using the computer subroutines "DECOMP" to perform Gaussian elimination and "KQUAD" to perform the inverse integration. Both subroutines "DECOMP" and "KQUAD" are in a IBM-3081D computer. DECOMP solves a linear system of equations by Gaussian elimination; KQUAD integrates real functions of one variable over a finite interval, using an adaptive quadrature scheme based upon Gauss-Kronrod algorithms.

These two subroutines all deal with real functions and variables, but the present problem involves complex functions of the complex variable s. Therefore, we do the following work for the computer:

(i) For the program "DECOMP":

Basically, we solve a linear system of equations in matrix form as

$$\mathfrak{A}\,\mathfrak{X} = \mathfrak{C} \tag{3.4}$$

where $\mathfrak{A}$, $\mathfrak{X}$, and $\mathfrak{C}$ are all complex, we can decompose them as follows

$$(a + ib)(x + iy) = (c + id)$$

$$\rightarrow \quad (ax - by) + i(bx + ay) = (c + id) \tag{3.5}$$

This equation may be written as

$$\begin{bmatrix} a & -b \\ b & a \end{bmatrix} \begin{Bmatrix} x \\ y \end{Bmatrix} = \begin{Bmatrix} c \\ d \end{Bmatrix} \tag{3.6}$$

Equation (3.6) suggests that, instead of inputting a 6x6 complex number matrix, we input a 12x12 real number matrix.

(ii) For the program "KQUAD"

We integrate functions like:

$$g(\xi,\eta) = \int_{-\infty+ic}^{+\infty+ic} \tilde{g}(s,\eta)\exp(-is\xi)ds, \tag{3.7}$$

where $g(\xi,\eta)$ is a real function, but $\tilde{g}(s,\eta)$ is a complex function, Therefore, for a real variable solution, eventually, we do the integration

$$g(\xi,\eta) = \mathrm{Re}\left[\int_{-\infty+ic}^{+\infty+ic} \tilde{g}(s,\eta)\exp(-is\xi)ds \right], \tag{3.8}$$

where Re[ ] means "take the real part of the function in the square brackets", Equation (3.8) can also be rewritten in terms of the real variable u as

$$g(\xi,\eta) = \int_{-\infty}^{+\infty} \mathrm{Re}\left[\tilde{g}(u-ic,\eta)\exp\left(-i(u-ic)\xi\right)\right]du. \tag{3.9}$$

The Equation (3.9) indicates that, instead of integrating a complex

function, we can just take the real part of the integrand and translate the integral path by a distance c parallel to the real axis to avoid the singularity at the origin, and then integrate it by computer.

Chpater 4

Parametric Study

4.1 Asperity Parameters and Critical Depth

The asperity parameters consist of asperity speed V, pressure P, and contact area a. The coefficient of Coulomb friction μ_f relates the normal force and the friction force. The friction force generates both the mechanical portion and the thermal portion of the stress state. Its rubbing speed (V) influences the thermal input. It is readily conceivable that, at low rubbing speed, the mechanical portion of the stress dominates. The static case of V=0 is indeed the limiting case. Therefore, at high speed, the thermal stress prevails (see Figure 2). Without loss of generality, the distribution of asperity pressure is assumed to be UNIFORM, for mathematical simplicity. For the effect of non-uniform pressure distribution, see the results of Ju and Huang [9,10], it was shown that the assumption of uniform distribution of asperity pressure will result in stresses 40% less than those from three-dimensional non-uniform distribution of pressure [10,12,13]. However, it is adequate to use this assumption in the study of interaction among various parameters without actually predicting the stress level for fracture initiation.

We shall designate η_{cr} as the critical depth where maximum principal thermal tensile stress occurs for single material or for the coating as a single material, and η_{max} that for the coated medium.

For various parameters and coating thickness, the anal[illegible] principally will locate the depth η_{max}. This depth is dep[illegible]ent on the material and the coating thickness . From the set $\{\eta_{max}\}$, the worst case corresponding to one with the highest maximum thermal tensile stress is important to the designer. Such a worst case is related to the critical depth η_{cr}.

The depth η_{cr}, for a single wear material, where maximum principal thermal tensile stress occurs is shown in Figure 5. In this figure, the solid line represents the theoretical η_{cr} as a function of Peclet number. The analytical computation of this solid line is from the solution of thermal stresses for a single material (see Appendix A). For the numerical result, we select two materials, Stellite III and Aluminum Oxide, as the test materials. Varying the Peclet number ($R=Va/\kappa$) for both is therefore accomplished with varying the asperity traversing speed. The principal thermal stresses in the trailing edge of the asperity is calculated for changing depths from the wear surface. Then the critical depth η_{cr} is obtained where the maximum principal thermal tensile stress occurs. Hence, we have the relationship between the η_{cr} and the Peclet number for the two-dimensional case.

The critical depths for three other materials Aluminum (Al), Silicon Carbon (SiC), and Zirconium (Zr) are computed for the same asperity speed of 15 ms^{-1}, and the same asperity width of 0.254 mm. For each of these materials, the material properties are different from those of the test materials. It is shown in Figure 5, the critical

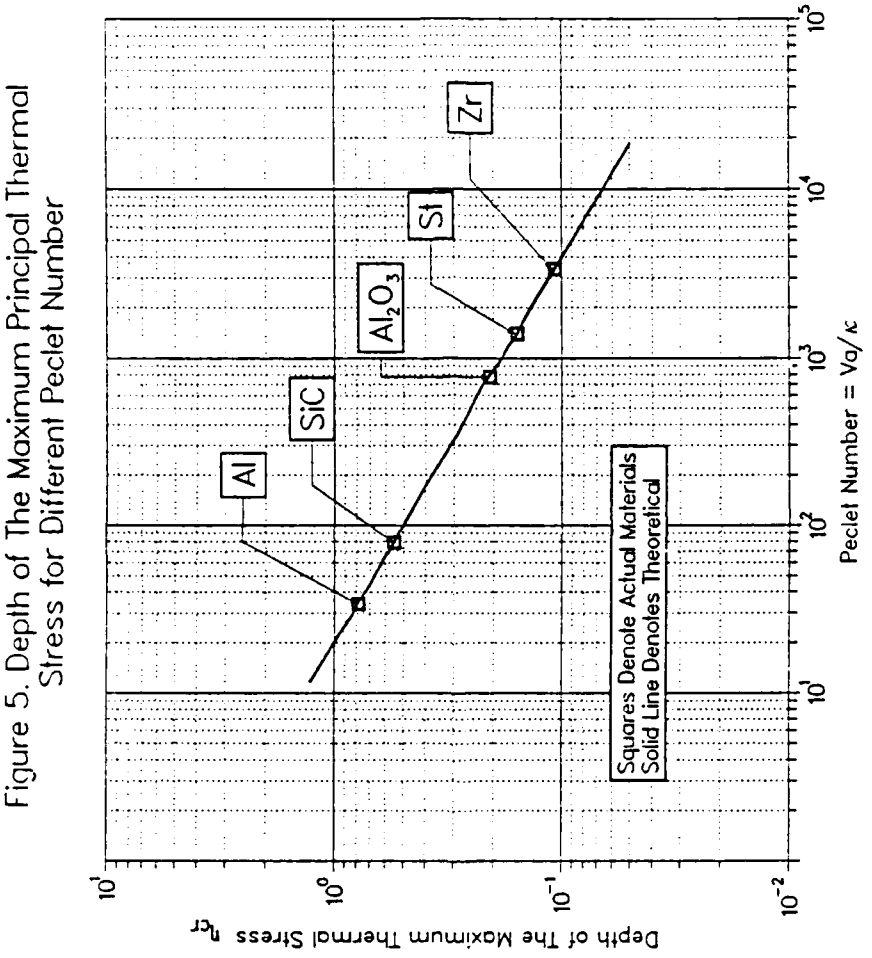

Figure 5. Depth of The Maximum Principal Thermal Stress for Different Peclet Number

depth η_{cr} of each material falls on the theoretical line. This illustrates that the critical depth, for a single asperity excitation over a single wear material, depends predominantly upon the Peclet number, $R=Va/\kappa$. From Figure 5, the relation between the η_{cr} and the Peclet number for the two-dimensional case can be expressed by a simple equation as:

$$R(\eta_{cr})^{2.275} = 20.4368 \tag{4.1}$$

Figures 6 and 7 show, as functions of depth, the thermal principal stress (σ^I) and the temperature gradient for Alumimum and Stellite III, respectively. From a physical point of view, if the asperity velocity and contact width are constant, higher Peclet number means the diffusivity is small. Hence, the speed of the heat transfer into the medium is slower, and the depth η_{cr} is moderately shallow. On the other hand, from a mathematical point of view, Equation (A.19) shows that, for higher Peclet number, the decay rates of the temperature gradient are greater. Therefore, the depth to reach the maximum principal thermal tensile stress will approach the free surface asymptotically as the Peclet number increases and vice versa. Figure 6 is for Aluminum and Figure 7 is for Stellite III, because the Peclet number for Stellite III ($R \cong 1400$) is larger than Aluminum ($R \cong 34$) for a given velocity, consequently, the $(\eta_{cr})_{Al}$ is larger than $(\eta_{cr})_{St}$. These two figures not only illustrate that the maximum principal stress occurs around the point where the temperature gradient begins to attenuate, but also imply the results of Figure 5. The principal thermal stress at various depth at the trailing edge of the asperity.

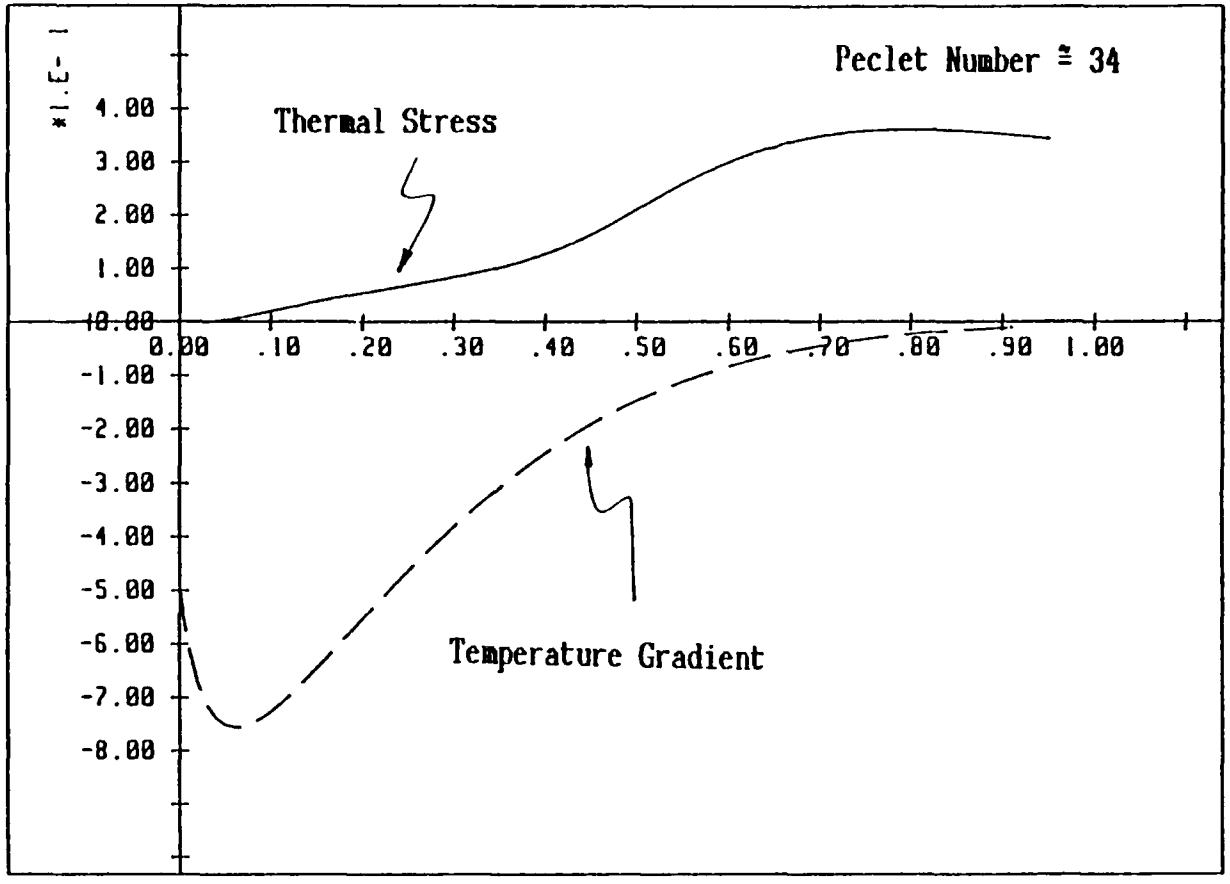

Figure 6. Thermal stress and temperature gradient vs. depth coordinate for aluminium.

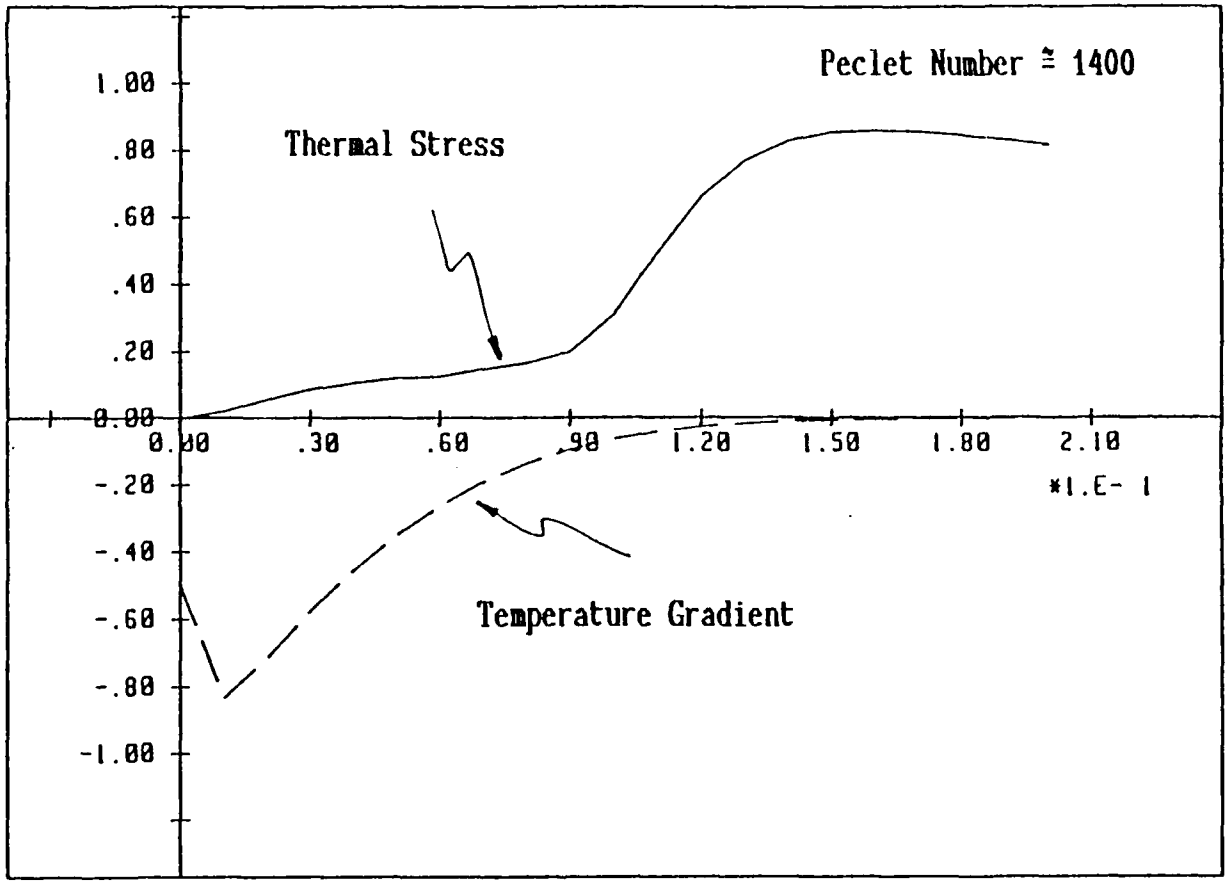

Figure 7. Thermal stress and temperature gradient vs. depth coordinate for Stallite III.

for different values of Peclet number, the non-dimensional stress in Figure 8 incorporates the material properties to yield material independent values. Therefore, in any given material, for a given Peclet number, we can obtain the critical depth η_{cr} from Figure 5 or Equation (4.1). The maximum thermal stress corresponding to a given Peclet number can be obtained for any material from Figure 8.

4.2 Material Parameters

As the emphasis of the paper is on the friction force and the rate of frictional work, the simple linear Coulomb law is used, $F_f = \mu_f F_n$, for analytical convenience. The rate of frictional work heats the surface layer of the wear medium to raise the surface temperature, which in turn increases the Coulomb coefficient μ_f with resulting further increase in friction force [22]. The present analysis avoids the iteration by using the maximum Coulomb's coefficient of friction to anticipate a steady state high temperature field. Equation (8) shown that the mass density (ρ) affects the stress field through the Mach number (M) and the thermal field through the thermal diffusivity ($\kappa = k/\rho c$). Since the Mach number is generally so small for this class of problems, the effect of the mass density is principally reflected through the thermal capacity (ρc), where c denotes the specific heat.

The mechanical constitutive coefficients and the coefficient of thermal expansion affect the thermal stress field through the material compliances and the thermal dilatation. Stiffer material and high thermal expansion are known to contribute toward higher thermal

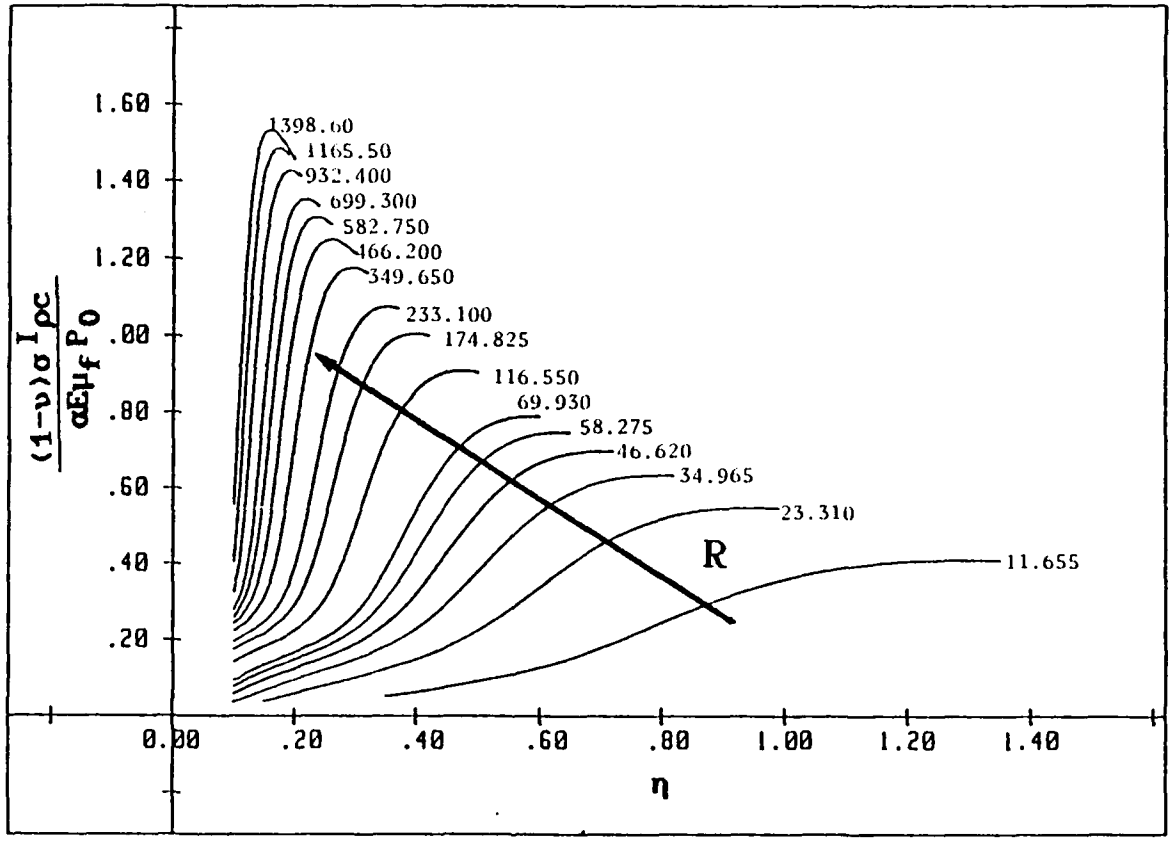

Figure 8. Principal thermal stress vs. depth coordinate for different Peclet number.

stresses. The effects of the thermal parameters ($k, \kappa, \rho c$ - conductivity, diffusivity and capacity) can be found from Ju and Huang [12] and Ju [13]. These references show that the thermal diffusivity is indeed a derivative thermal parameter. It is the individual value of the thermal capacity, the thermal conductivity or their combination that determines the thermal field, and the stress field that leads to thermo-mechanical cracking of the wear material.

Hence, for the mechanical and thermal impedance matching between the surface layer and the substrate, we will therefore consider the differences in mechanical constitutive coefficient, coefficient of thermal expansion, thermal conductivities and thermal diffusivities.

4.3 Coating Layer Thickness Effects

The estimate of thermo-mechanical cracking from high speed asperity excitation in the layered medium is more complicated than that of a single wear material. The latter, as shown by Ju and Huang [9,10,12], predicts the fracture initiation in hard wear material to be cohesive failure at the depth η_{max}, where the maximum principal thermal stress occurs. For layered media, the initiation may occur: (1) inside the surface layer, (2) in the substrate, both through cohesive failure, or (3) at the coating/substrate interface through shear delamination. Ju and Chen [8] have shown that, for a thick coating layer, with thickness of the order of the asperity size, the critical stress will be inside the coating at the thermal layer. The present paper thus will address the stress states in the surface layer as well as in the substrate for

various coating thicknesses, taking into consideration the effects of mechanical and thermal impedance mismatchings. The following results are based on Stellite III as test material for both surface layer and the substrate.

4.3.1 Effects of Differences in Mechanical Impedance

The effects of both the elastic coefficient and the coefficient of thermal expansion are mechanical. In the solutions for thermal stresses, they appear as a group, $\alpha E/(1-\nu)$, which defines the mechanical impedance for both the surface layer and the substrate.

Figure 9 illustrates the depths η_{max} of maximum principal thermal stresses, as a function of the coating thickness based upon a given substrate property. In this figure, the substrate material properties are constants and the mechanical properties of the surface material are considered as variables. An increase in value of the dimensionless parameter $\Pi_M = [\alpha E/(1-\nu)]_I \; / \; [\alpha E/(1-\nu)]_{II} = 0.2,\ 0.5,\ 2.0$ and 5.0 indicate, respectively, two softer surface layers, and two harder surface layers. If coating thickness less than the depth η_{cr} of the coating material (for our case, it is assumed $\eta_{cr} = 0.16$), the maximum thermal principal stress occurs in the substrate. The η_{max} will slightly change, depending upon the value $\alpha E/(1-\nu)$ of the surface layer. If Π_M for the surface is larger than Π_M for thesubstrate, then the surface layer is harder than the substrate. Therefore the displacement gradient in the surface layer will become larger than the substrate. From Equation (2.3), indicates that if the displacement

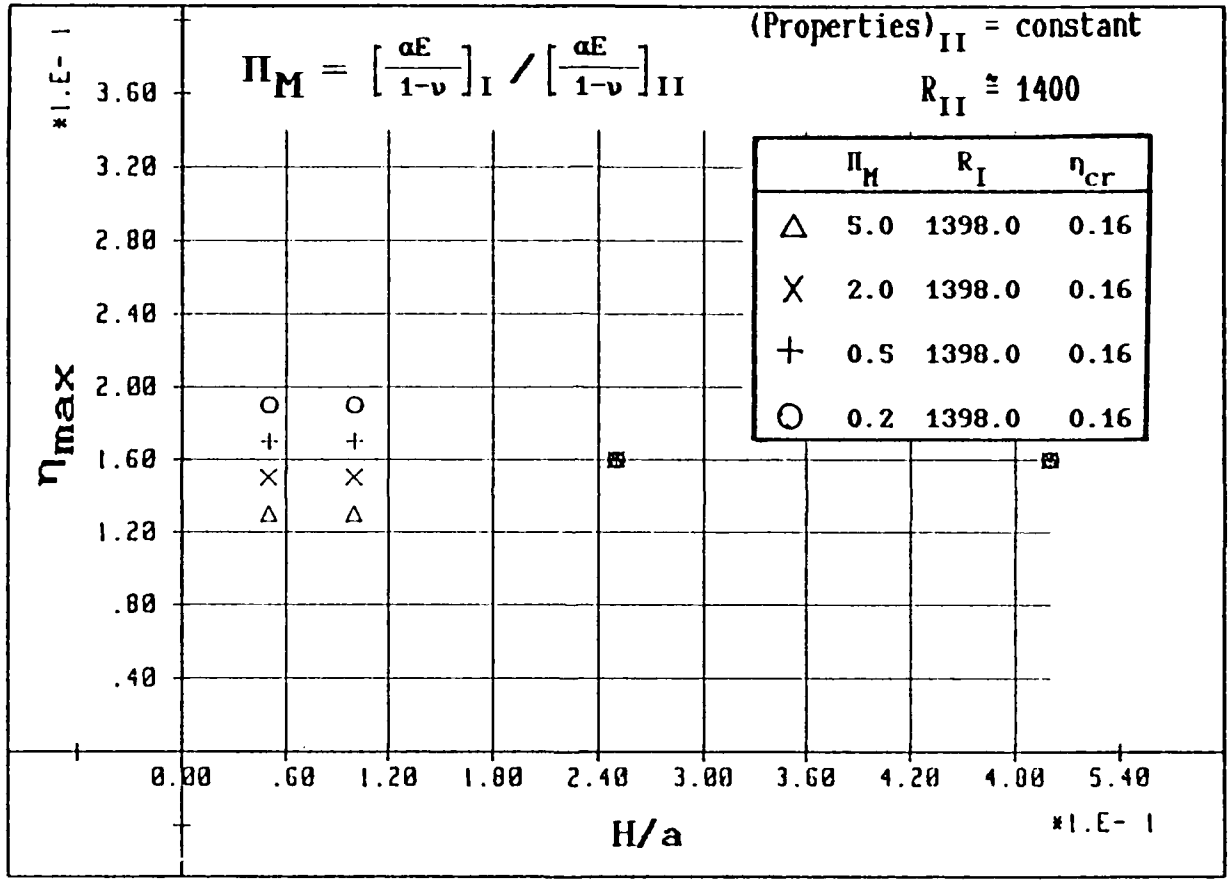

Figure 9. η_{max} vs. layer thickness for varying mechanical properties.

gradient of a surface layer for a layered medium is larger than for a single material, then the temperature term is not affected by a change in mechanical properties, and therefore the position where the maximum principal thermal stress occurs will be shallower than for a single material . Conversely, it will be deeper than for single material. For coating thickness larger than η_{cr}, because we didn't change the Peclet number for surface layer, the η_{max} will be the same as treating the surface as a single material. Consequently, the layered medium is similar to the single. This implies that, whether a layered medium is like a single material or not, it depends upon the Peclet number of material. When the Peclet number is large, the η_{cr} is small, and then only a very thin coating can be treated as single material.

In Figure 10 and Figure 11, the surface material is fixed. Figure 10 illustrates the maximum principal thermal stress in the surface layer, σ_I^T, as a function of the coating thickness. The values of the dimensionless parameter Π_M = 0.5, 1.0 and 2.0 indicate, respectively, a harder substrate, same material and a softer substrate. For coating thickness less than the depth η_{cr}, the maximum thermal stress in the coating layer occurs in the neighborhood of the coating/substrate interface. With increase of the coating thickness, greater than the depth η_{cr}, the maximum thermal stress is in the neighborhood of the depth η_{max} with diminishing effect of the substrate. It is noticed that, after a value of $2\eta_{cr}$, the result is no different from that of a single material. Figure 9 shows the corresponding maximum principal thermal stresses in the substrate, σ_{II}^T, as a function of the coating thickness. Since η_{max} for thin coating is inside the substrate, the

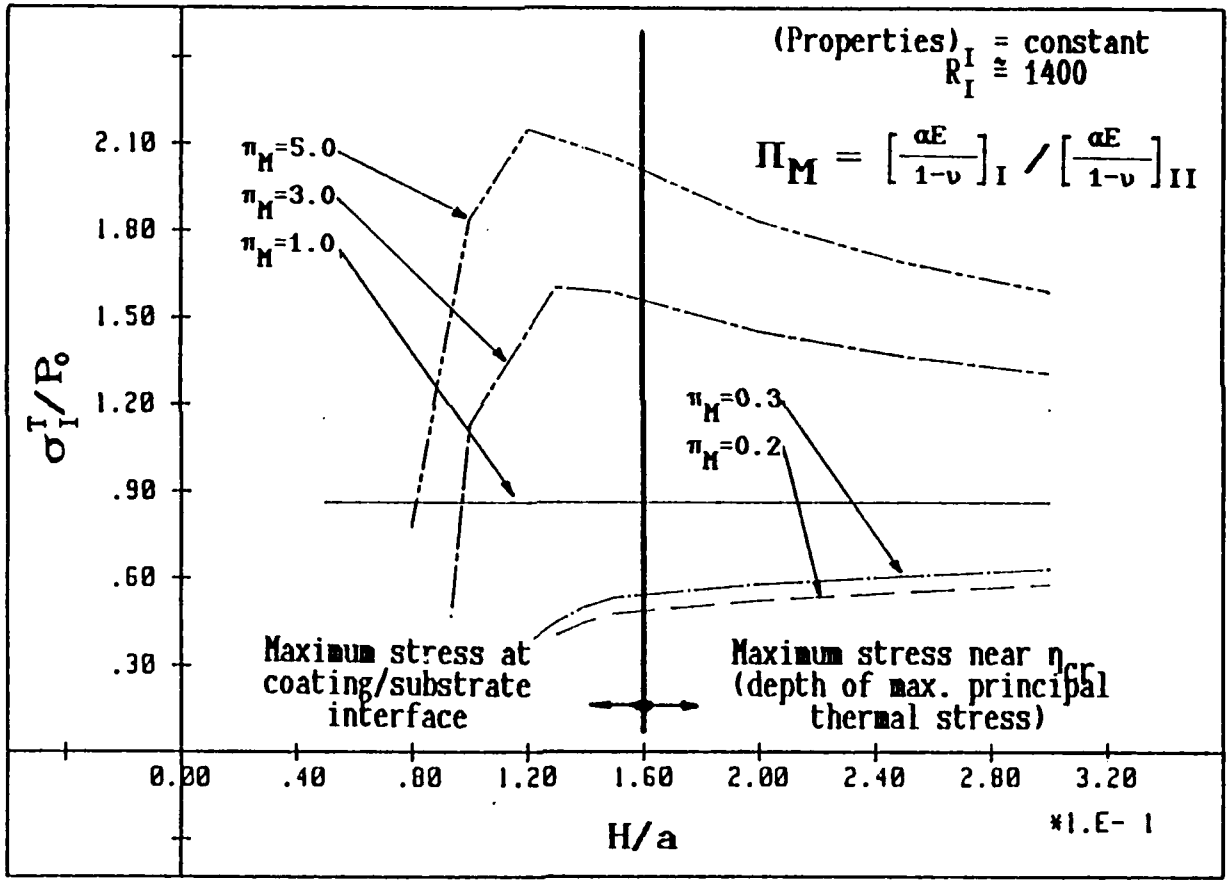

Figure 10. Maximum principal stress in coating layer vs. coating thickness for different mechanical mismatch.

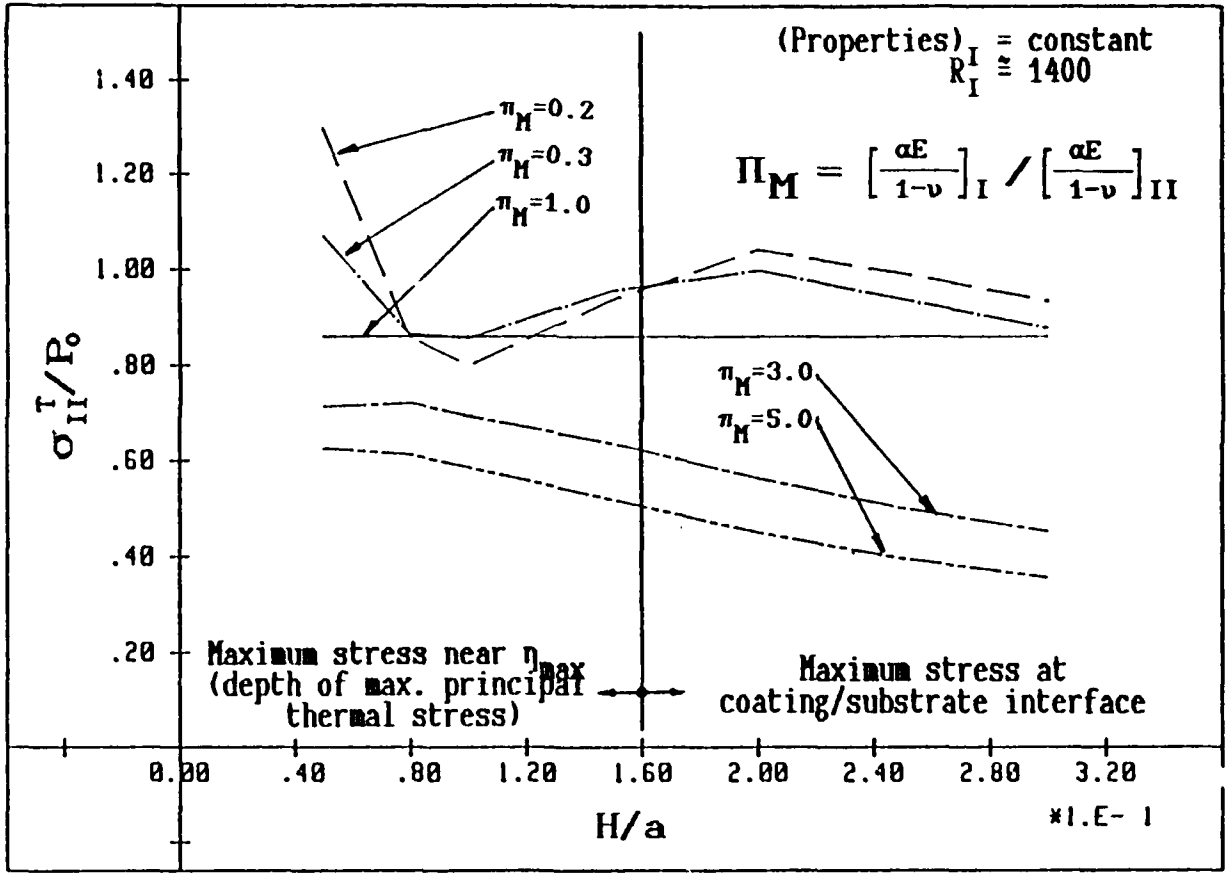

Figure 11. Maximum principal stress in substrate for different mechanical mismatches.

maximum thermal stress will occur therein. The maximum substrate stress for coating thicker than the depth η_{cr} will be at the coating/substrate interface. The prediction of fracture initiation must depend on the cohesive strength of individual materials of the coating and the substrate.

4.3.2 Effects of Differences in Thermal Properties

Figure 12 shows the depths of maximum principal thermal stresses, η_{max}, as a function of the coating thickness based upon a given substrate material property, with conductivity ratio, $\Pi_k = k_I/k_{II}$, as the parameter. The values of $\Pi_k = 0.2$, 0.5, 2.0 and 5.0 indicate, respectively, two more insulating surface layers up to two more conductive surface layers. In this figure, we do not vary the substrate material properties. When the coating thickness is less than η_{cr}, the value of η_{max} will slightly change, due to the conditions of the surface layer. For the more conductive surface layer, because more heat can be dumped into the substrate, the η_{max} will be deeper. Converserly, η_{max} will be shallower when we have a more insulating surface. Because the Peclet number is not changed, when the coating thickness is larger than η_{cr}, the η_{max} will be equal to η_{cr}.

Figure 13 shows the maximum principal thermal stresses in the surface layer, σ_I^T, as function of the coating thickness, with the conductivity ratio, $\Pi_k = k_I/k_{II}$, as the parameter. Similar to the case of mechanical mismatch, the maximum stresses in thick coatings are at the depth η_{cr} and approach that of the single wear material.

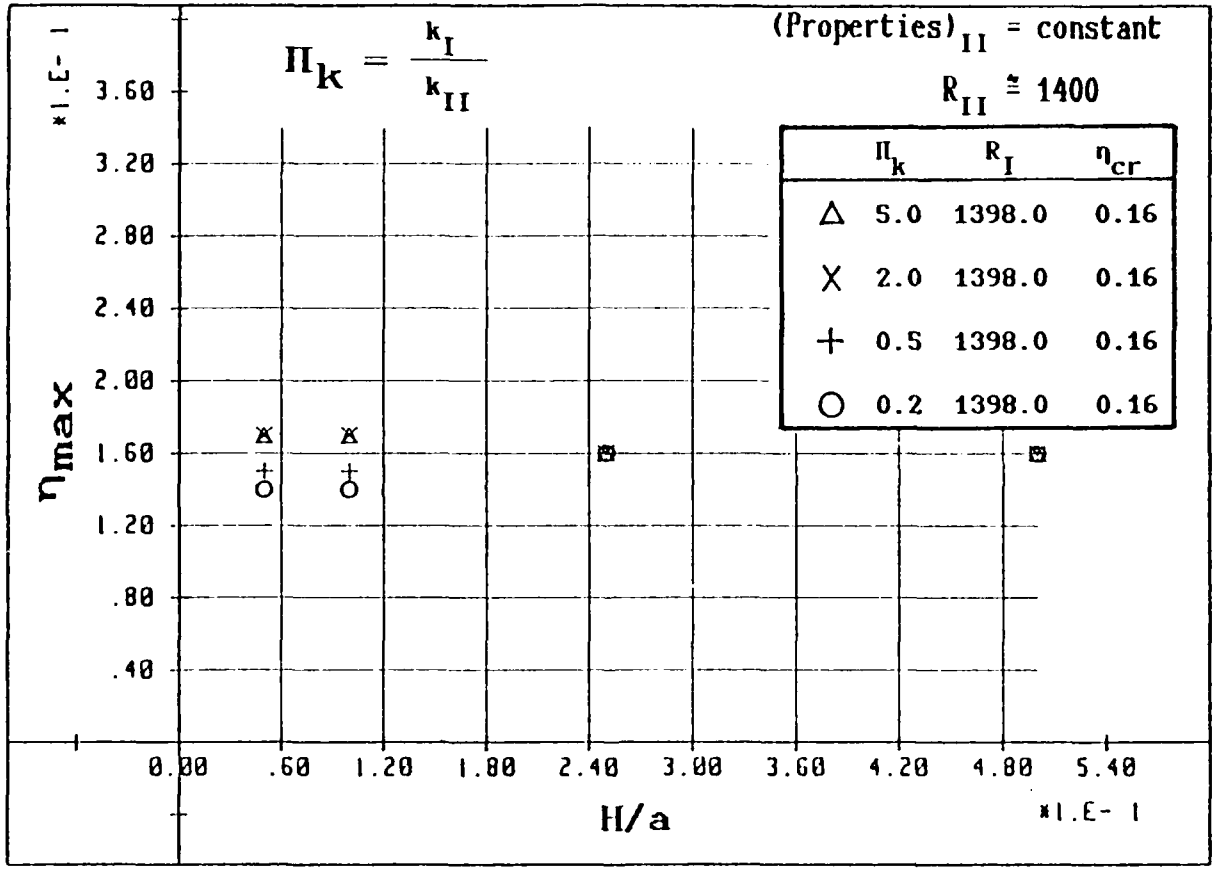

Figure 12. η_{max} vs. coating thickness for different mismatches in thermal conductivity.

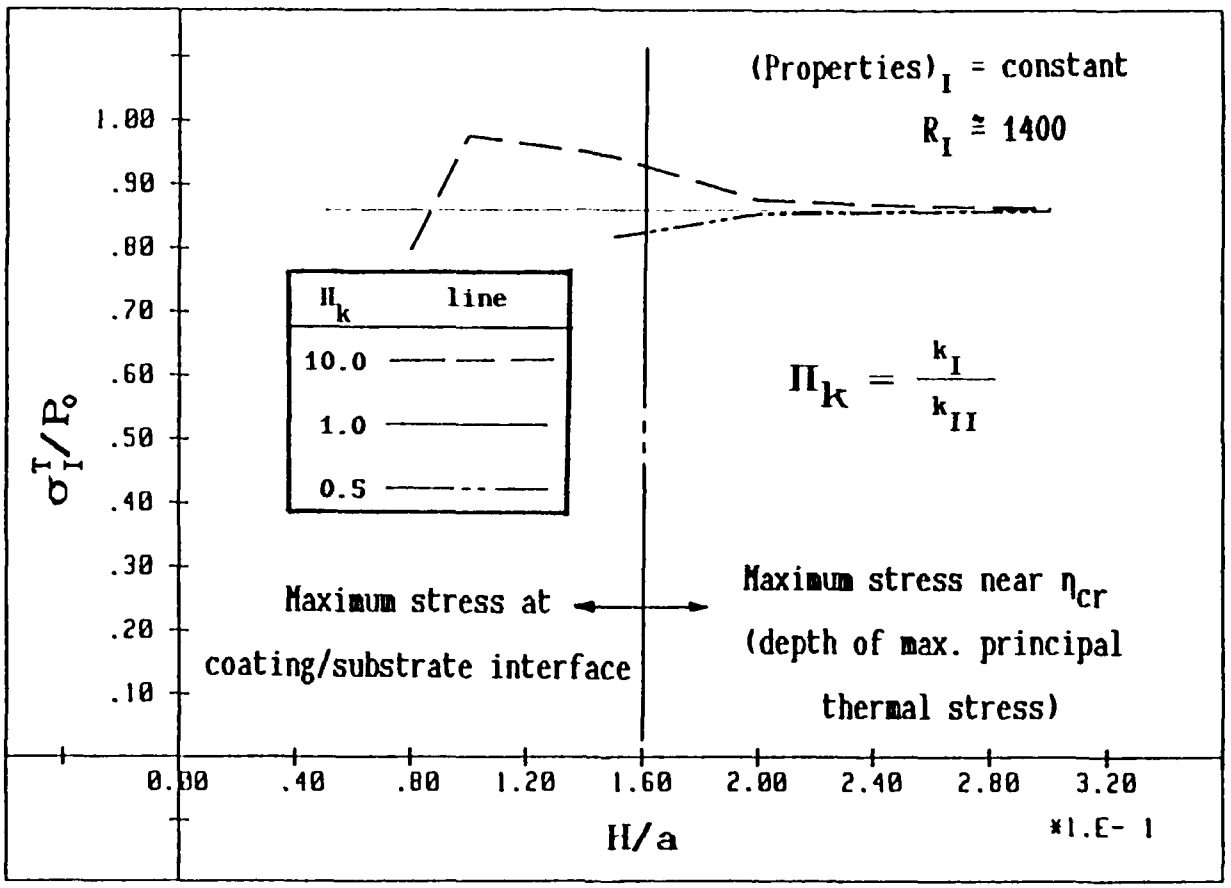

Figure 13. Maximum principal stress in coating layer vs. coating thickness for different mismatches in thermal conductivity.

When the substrate is less conductive, $\Pi_k = 10.0$, the therm stress is higher in the surface layer, especially on the coating substrate $\Pi_k = 0.5$; more heat is readily transferred to the substrate. The thermal stress is correspondingly reduced. The maximum principal thermal stresses in the substrate has a similar trend, as shown in Figure 14.

Figure 15 (substrate material properties are constant) illustrates that when we change the surface material's Peclet member, the η_{max} will be changed significantly. Nevertheless, there is a general rule to help us to determine where η_{max} is. We have used the rule for the previous two cases. That is, when the coating thickness is less than the η_{cr} for the surface layer as a single material, the η_{max} for layered media will be determined by the substrate material properties, but we shall consider the effects of surface layer. At this moment, when $\Pi_{\rho c} < 1$, it means the surface temperature gradient is larger than the substrate. Therefore, from Equation (2.3), the η_{max} is slightly larger than η_{cr} which is defined by the coating material. Converserly, the η_{max} is smaller than η_{cr}. When the coating thickness is larger than η_{cr} for the surface as a single material, the η_{max} will be determined by the surface material properties. Similarly, Figure 16 shows that, when the surface material properties are constant, then η_{max} has the same tendency.

Figure 17 illustrates a combined curve for maximum principal thermal stresses, indicating that the maximum stress for thin coating is inside the substrate, but it is in the surface layer for thick coatings. In both cases, the stresses are evaluated at the depth η_{max}.

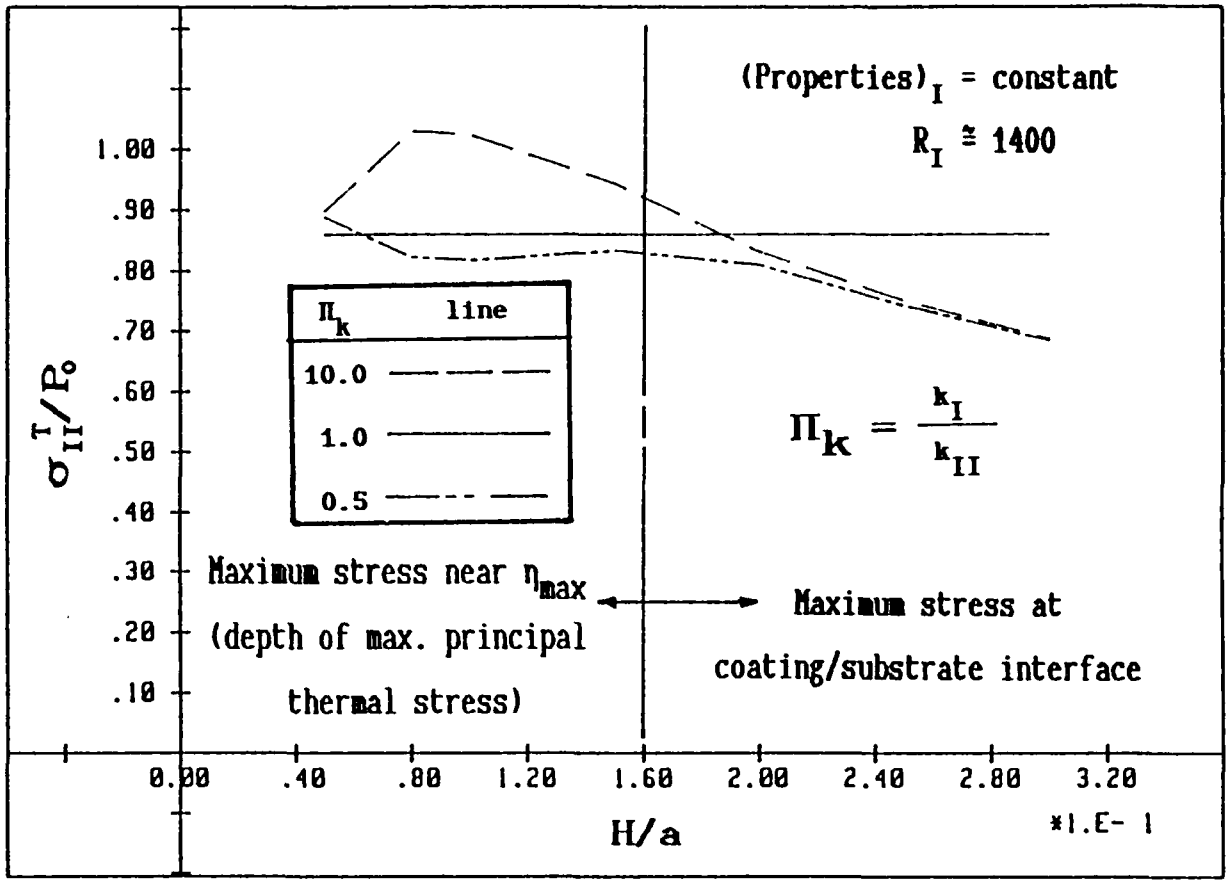

Figure 14. Maximum principal stress in substrate vs. coating thickness for different mismatches in thermal conductivity.

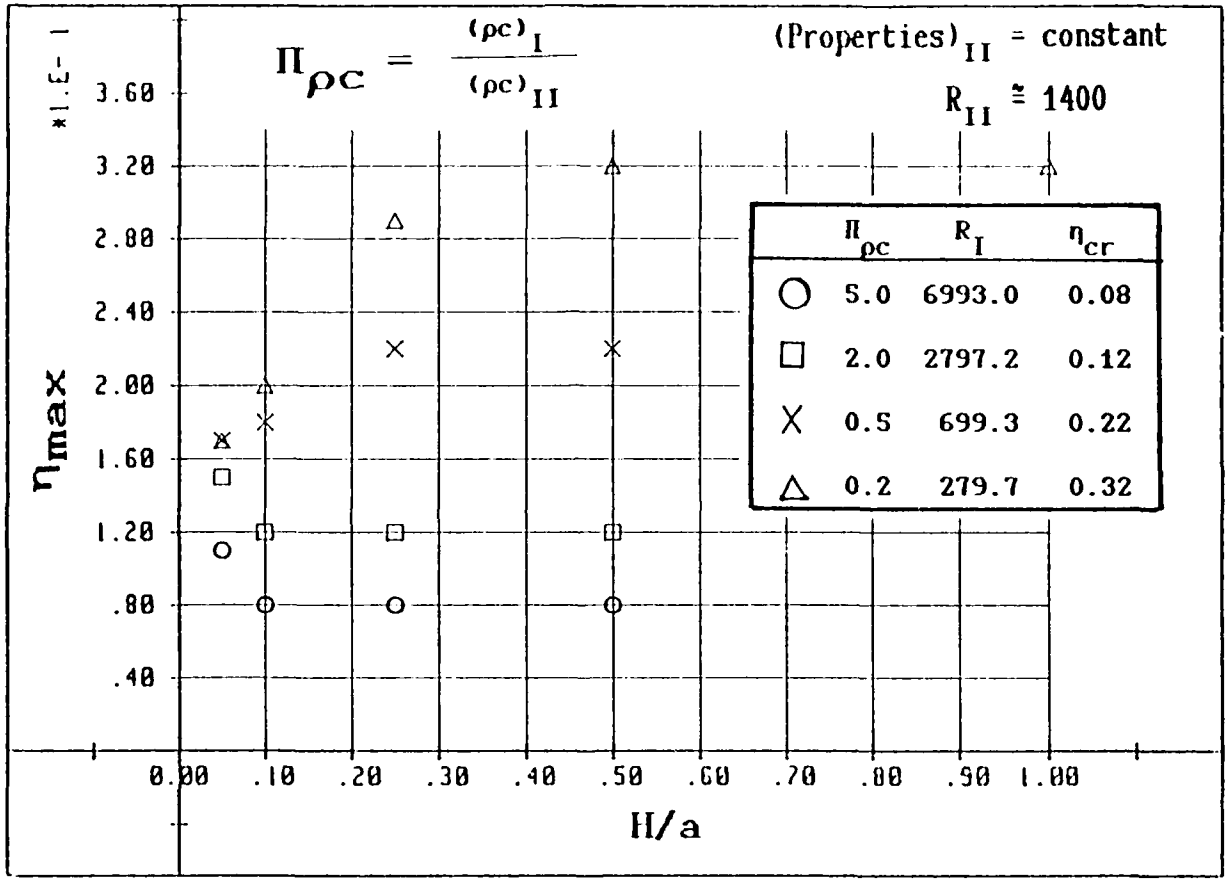

Figure 15. η_{max} vs. coating thickness for different mismatches in thermal capacity from different coating material.

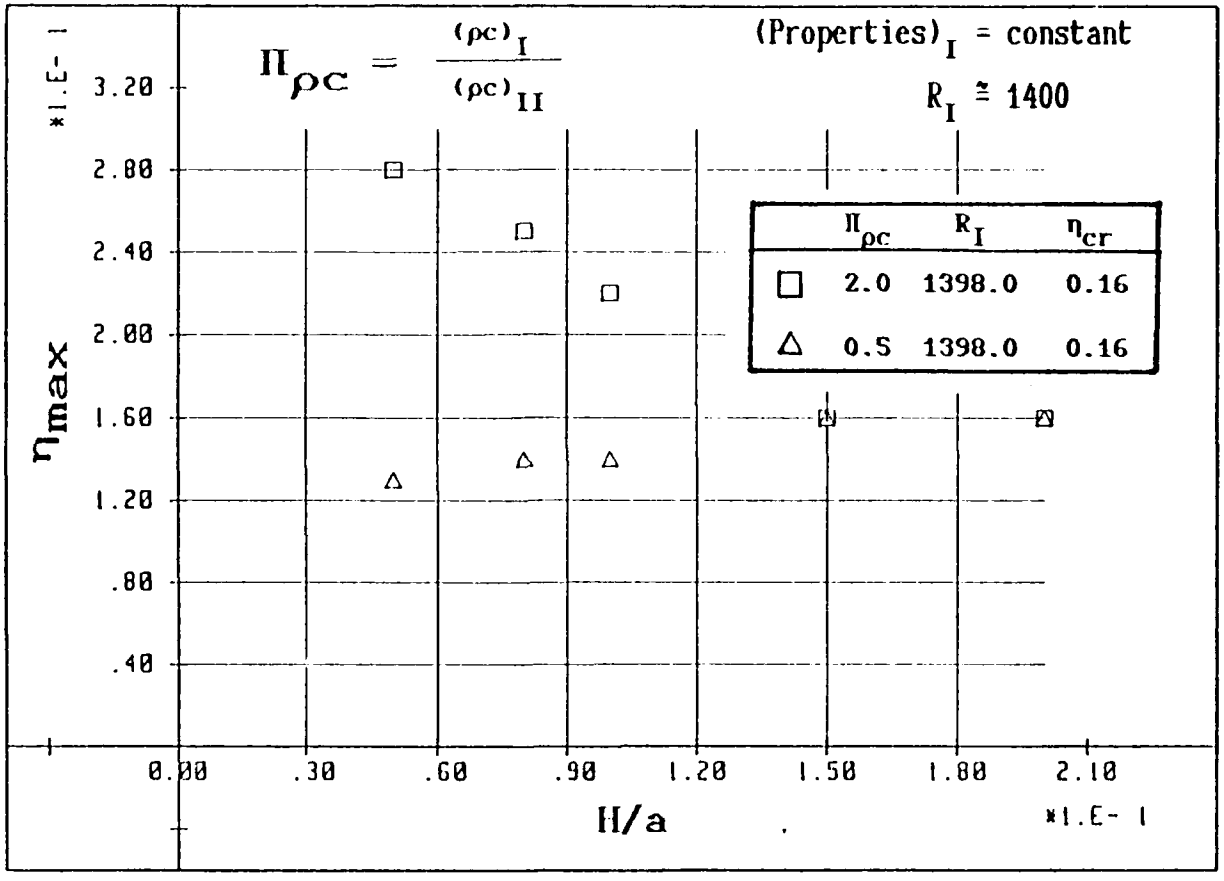

Figure 16. η_{max} vs. coating thickness for different micmatches in thermal capacity from different substrate material.

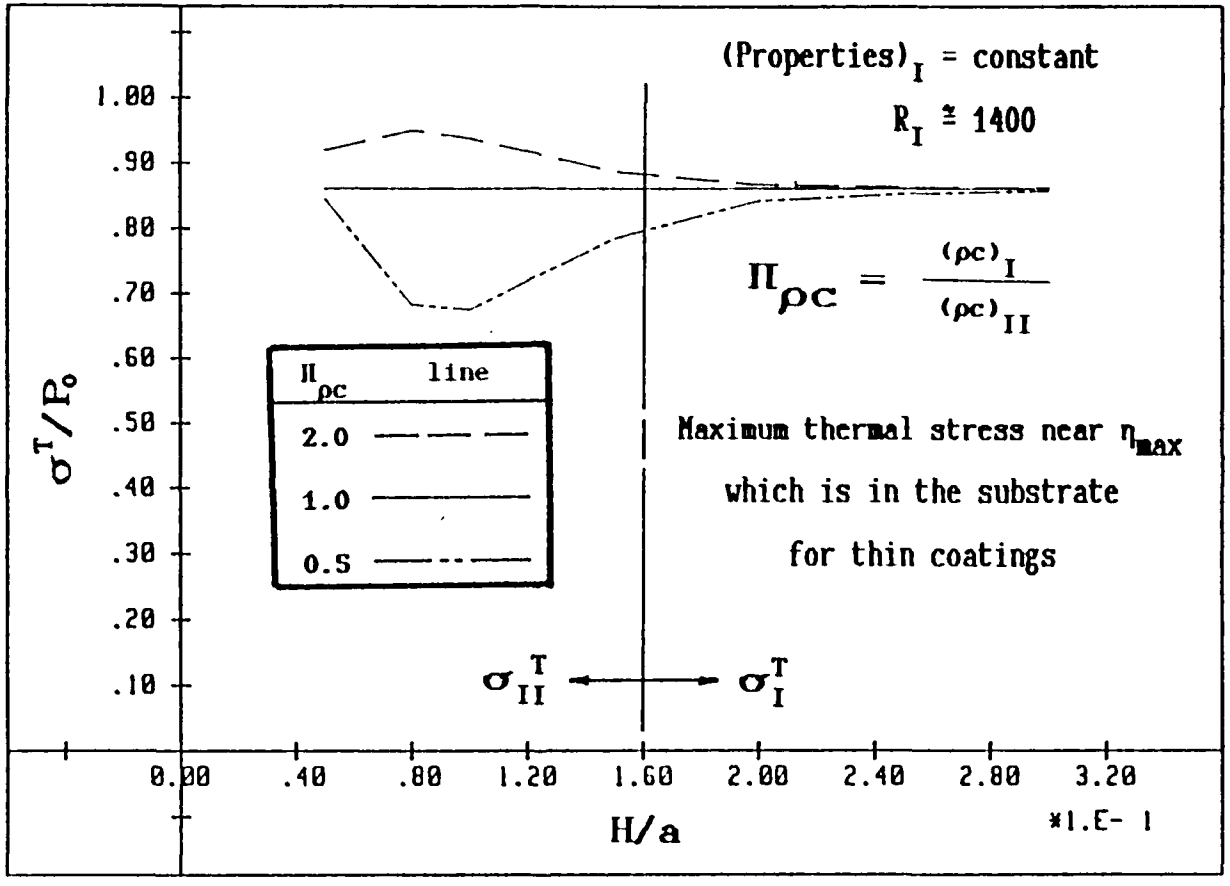

Figure 17. Maximum principal stress vs. coating thickness for different mismatches of thermal capacity.

4.3.3 Shearing Stress at the Coating/Substrate Interface

Because of the asymmetrical distribution of the temperature gradient, the direction of the maximum temperature gradient is as anticipated, not perpendicular to the wear surface. The resulting value of shearing stress at the coating/substrate interface is not to be ignored. In Figure 18, the curve for $\Pi_k = 1.0$ can be considered as the shearing stress at different depths from the wear surface for a single wear material. The worst case shows the maximum shearing stress at almost 30% of the maximum principal stress. The value is significant in designing the coating/substrate bonding strength to avoid shear delamination. The difference in thermal conductivities of the coating and the substrate is shown to affect the interface shearing stress for thin coating layers, If the coating/substrate bonding of a thin coating is a primary consideration, the substrate may purposely, by design, be less conductive.

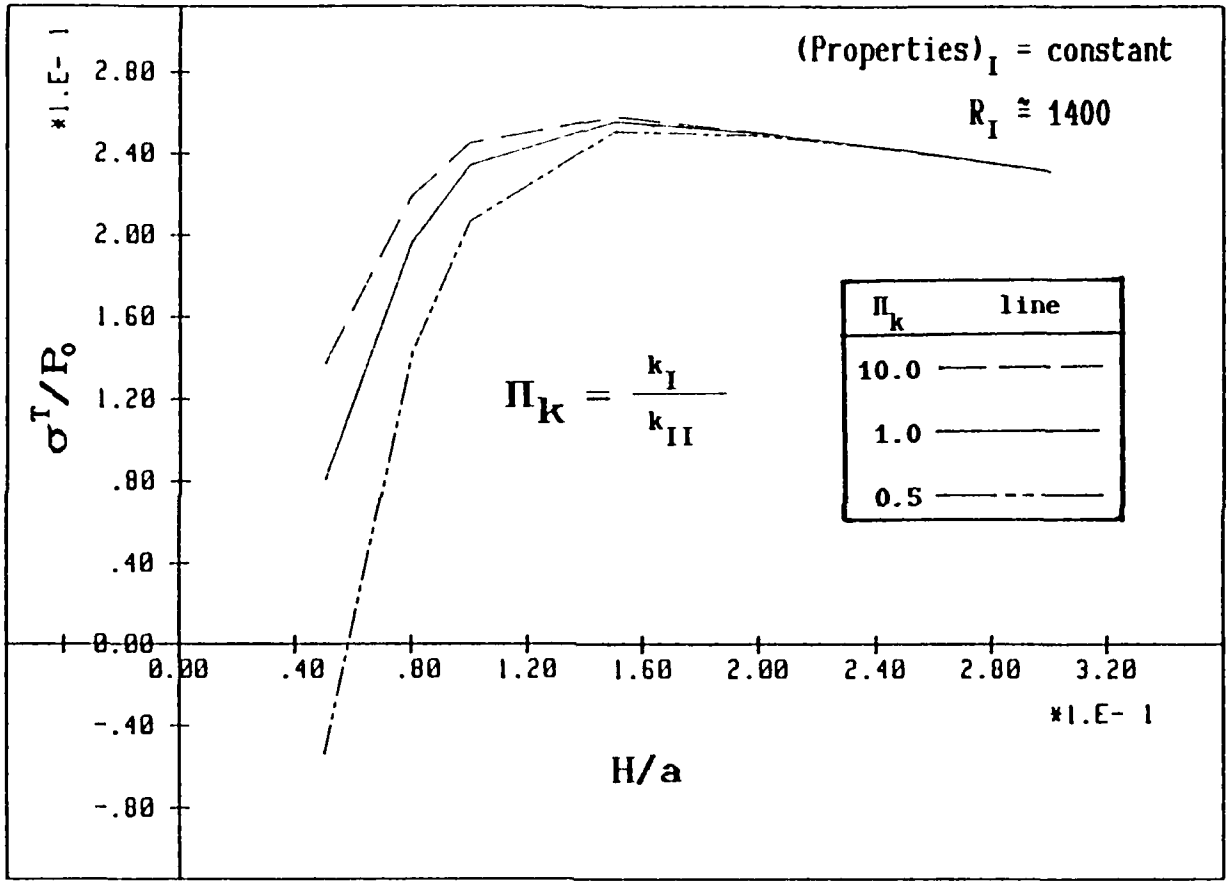

Figure 18. Interface shearing stress vs. coating thickness for different mismatches in thermal conductivity.

Chapter 5

Conclusions

The paper demostrates the significant effects of the Peclet number and the material mismatch between the surface layer and the substrate in high speed asperity excitation. Principally it is the critical depth η_{cr} at which the thermal tensile stress reaches a maximum. Peclet number is proven to dominate the determination of the critical depth, which is obtained from maximizing the thermal tensile stress in the vicinity of the asperity trailing edge. In other words, the asperity velocity, the asperity size, and the material diffusivity are the principal three factors that dominate the critical depth. A simplified depth η_{cr} as Equation (4.1) can be approximated. From this result, the maximum tensile stress in its alternate non-dimensional form can be obtained for all wear materials. Since the numerical empirical equation, Equation (4.1), has been demonstrated not to depend on the other material properties nor the magnitude of asperity excitation, the coefficient and the exponent are therefore constants in the two-dimensional model. It is, however, expected that the coefficient and the exponent in Equation (4.1) would be function of the aspect ratio of the asperity contact area. The work is under investigation with a three dimensional formulation.

The critical depth η_{cr} is important in the layered media analysis. It was shown by Ju and Chen [8] that the layer thickness is in the neighborhood of η_{cr}, the thermo-mechanical stress state is most damaging.

On the other hand, the highest stress occurs when the coating thickness is in the neighborhood of the η_{cr}, regardless of the differences in mechanical or thermal properties. As the coating thickness increases to more than the critical depth η_{cr} for the coating as asingle material, there is little effect of the substrate on the maximum thermal stress in the coating layer. Hence, if a thick coating is permissible and if the asperity size can be statistically ascertained, a properly chosen coating layer large than η_{cr} for coating material can be estimated to insure the improvement on wear resistance for materials such as composites. For thermal stress analysis of a layered media, in order to study the impedance matching of the surface layer and the substrate, it is adequate to consider the thermal conductivity (k), and the thermal capacity (ρc), while the effects of their differences are negligible for thick coatings; the effects on thin surface coating are important. Basically, substrates of low mechanical properties, higher thermal conductivity and capacity will result in lower stresses in both surface layer and the substrate. The initiation of the cracks will occur wherever the stress level surpasses the cohesive strength of the respective material. The critical locations in the surface layer or in the substrate depend on the coating thickness relative to the η_{cr}.

The shearing stress at the surface layer/substrate interface is by no means trivial, depending again on the surface coating thickness. The interface shear reaches a maximum when the coating thickness is in the neighborhood of η_{max}. This knowledge is important for the design of bonding of the surface coating. Any shear crack, resulting from the

shear delamination at the interface could cause further ext ion at repeated asperity excitations.

Appendix A

The Equations and Solutions for Single Material

In this Appendix we present the solutions for the zeroth order Approximation.

(I) Mechanical Stress Field:

$$N^2\frac{\partial^2 u}{\partial \xi^2} + (N^2-1)\frac{\partial^2 v}{\partial \xi \partial \eta} + \frac{\partial^2 u}{\partial \eta^2} = 0, \tag{A.1}$$

$$\frac{\partial^2 v}{\partial \xi^2} + (N^2-1)\frac{\partial^2 u}{\partial \xi \partial \eta} + N^2\frac{\partial^2 v}{\partial \eta^2} = 0, \tag{A.2}$$

$$\sigma_{\xi\xi} = \frac{\mu}{P_0}\left[N^2\frac{\partial u}{\partial \xi} + (N^2+2)\frac{\partial v}{\partial \eta} \right], \tag{A.3}$$

$$\sigma_{\xi\eta} = \frac{\mu}{P_0}\left[\frac{\partial v}{\partial \xi} + \frac{\partial u}{\partial \eta} \right], \tag{A.4}$$

$$\sigma_{\eta\eta} = \frac{\mu}{P_0}\left[(N^2+2)\frac{\partial u}{\partial \xi} + N^2\frac{\partial v}{\partial \eta} \right]. \tag{A.5}$$

The boundary conditions, the regularity conditions are:

$$\sigma_{\eta\eta} = \mu_f P(\xi) \quad \text{at } \eta = 0, \quad -1 \le \xi \le 1, \tag{A.6}$$

$$\sigma_{\eta\eta} = \begin{cases} -P(\xi) & -1 \le \xi \le 1 \qquad \eta = 0 \\ 0 & -1 \ge \xi \text{ and } \xi \ge 1 \quad \eta = 0 \end{cases}, \tag{A.7}$$

$$\sigma_{\xi\xi},\ \sigma_{\xi\eta},\ \sigma_{\eta\eta} \to 0 \text{ as } \quad \xi^2+\eta^2 \to \infty, \tag{A.8}$$

$$\sigma_{\xi\eta} = \sigma_{\xi\eta}', \qquad \sigma_{\eta\eta} = \sigma_{\eta\eta} \quad \text{at } \eta = D, \tag{A.9}$$

$$u = u \ , \quad v = v \qquad \text{at } \eta = D. \tag{A.10}$$

The solutions are

$$\tilde{v} = a^*\exp(-\eta s) + c^*\eta\exp(-\eta s), \tag{A.11}$$

$$\tilde{u} = i\Big[a^*\exp(-\eta s) + \Big(\frac{2}{q} - 1\Big)\frac{1}{s}\, c^*\exp(-\eta s) + c^*\eta\exp(-\eta s)\Big], \tag{A.12}$$

$$\tilde{\sigma}_{\xi\xi} = \frac{\mu}{P_0}\, s\Big[2a^*\exp(-\eta s) + 2\Big(\frac{2N^2-1}{1 - N^2}\Big)\frac{1}{s}\, c^*\exp(-\eta s) + 2c^*\eta\exp(-\eta s)\Big], \tag{A.13}$$

$$\tilde{\sigma}_{\xi\eta} = \frac{\mu}{P_0}\, (is)\Big[-2a^*\exp(-\eta s) - 2\Big(\Big(\frac{1}{q} - 1\Big)\frac{1}{s} + \eta\Big)c^*\exp(-\eta s)\Big], \tag{A.14}$$

$$\tilde{\sigma}_{\eta\eta} = \frac{\mu}{P_0}\, s\Big[-2a^*\exp(-\eta s) - \frac{2}{qs}\Big(c^*\exp(-\eta s) - 2c^*\eta\exp(-\eta s)\Big], \tag{A.15}$$

where

$$q = 1 - N^2,$$

$$a^* = \frac{\tilde{P}P_0}{2\mu}\Big[1 - i\mu_f\Big],$$

$$c^* = \frac{i\mu_f\tilde{P}P_0}{2s\mu} + a^*\Big(1 - \frac{1}{q}\Big)\frac{1}{s},$$

$$\tilde{P} = \frac{2\sin(s)}{s} \quad \text{for uniform unit pressure in the contact region } -1 \le \xi \le 1.$$

(II) Temperature Field

The governing equation are:

$$\frac{\partial^2\phi}{\partial\xi^2} + \frac{\partial^2\phi}{\partial\eta^2} = R\,\frac{\partial\phi}{\partial\xi}. \tag{A.16}$$

The boundary conditions, the regularity conditions are:

$$-\frac{\partial\phi}{\partial\eta} = Q^*(\xi) = \begin{cases} -Q(\xi) & -1 \le \xi \le 1 \quad \eta = 0 \\ 0 & -1 \ge \xi \text{ and } \xi \ge 1 \quad \eta = 0 \end{cases}, \tag{A.17}$$

$$\phi \to 0, \qquad \text{as } \xi^2+\eta^2 \to \infty, \tag{A.18}$$

The solution is:

$$\tilde{\phi} = A' \exp(-\sqrt{s^2 - \iota Rs}\ \eta), \tag{A.19}$$

where

$$A' = \tilde{Q}^*/F,$$

$$F = \sqrt{s^2 - \iota Rs}, \qquad Re[F] \ge 0,$$

$$\tilde{Q} = \frac{2\sin(s)}{s}, \quad \text{for uniform unit pressure for } -1 \le \xi \le 1.$$

(III) Thermal Stress Field

The governing equations are:

$$N^2\frac{\partial^2 u}{\partial \xi^2} + (N^2-1)\frac{\partial^2 v}{\partial \xi \partial \eta} + \frac{\partial^2 u}{\partial \eta^2} - \frac{b^2\gamma}{C_2^2}\frac{\partial \phi}{\partial \xi}, \tag{A.20}$$

$$\frac{\partial^2 v}{\partial \xi^2} + (N^2-1)\frac{\partial^2 u}{\partial \xi \partial \eta} + N^2\frac{\partial^2 v}{\partial \eta^2} - \frac{b^2\gamma}{C_2^2}\frac{\partial \phi}{\partial \eta}, \tag{A.21}$$

$$\sigma_{\xi\xi} = \frac{\mu}{P_0}\left[N^2\frac{\partial u}{\partial \xi} + (N^2+2)\frac{\partial v}{\partial \eta} - \frac{b^2\gamma}{C_2^2}\phi \right], \tag{A.22}$$

$$\sigma_{\xi\eta} = \frac{\mu}{P_0}\left[\frac{\partial v}{\partial \xi} + \frac{\partial u}{\partial \eta} \right], \tag{A.23}$$

$$\sigma_{\eta\eta} = \frac{\mu}{P_0}\left[(N^2+2)\frac{\partial u}{\partial \xi} + N^2\frac{\partial v}{\partial \eta} - \frac{b^2\gamma}{C_2^2}\phi \right]. \tag{A.24}$$

The boundary conditions, and the regularity conditions are:

$$\sigma_{\xi\eta} = 0 \quad \text{at } \eta = 0, \quad -1 \le \xi \le 1, \tag{A.25}$$

$$\sigma_{\eta\eta} = 0 \quad \text{at } \eta = 0, \quad -1 \le \xi \le 1, \tag{A.26}$$

$$\sigma_{\xi\xi},\ \sigma_{\xi\eta},\ \sigma_{\eta\eta} \to 0 \text{ as } \quad \xi^2+\eta^2 \to \infty, \tag{A.27}$$

The solutions are:

$$\bar{v} = A^* \exp(-\eta s) + C^*\eta \exp(-\eta s) + H \exp(-F\eta), \tag{A.28}$$

$$\bar{u} = \iota\left[A^* \exp(-\eta s) + \left(\frac{2}{q}-1\right)\frac{1}{s} C^* \exp(-\eta s) + \right.$$

$$\left. + C^*\eta \exp(-\eta s) - E_2 \exp(-F\eta) \right], \tag{A.29}$$

$$\bar{\sigma}_{\xi\xi} = \frac{\mu}{P_0} s\Big[2A^* \exp(-\eta s) + 2\Big(\frac{2N^2-1}{1-N^2}\Big)\frac{1}{s} C^* \exp(-\eta s$$

$$+ 2C^*\eta \exp(-\eta s) + E_3 \exp(-F\eta)\Big], \qquad (A.30)$$

$$\bar{\sigma}_{\xi\eta} = \frac{\mu}{P_0} (is)\Big[- 2A^* \exp(-\eta s) - 2(\frac{1}{q} -1)\frac{1}{s} C^* \exp(-\eta s) +$$

$$+ \eta C^* \exp(-\eta s) - E_4 \exp(-F\eta)\Big], \qquad (A.31)$$

$$\bar{\sigma}_{\eta\eta} = \frac{\mu}{P_0} s\Big[- 2A^* \exp(-\eta s) - \frac{2}{qs} C^* \exp(-\eta s) -$$

$$- 2C^* \eta\exp(-\eta s) + E_5 \exp(-F\eta)\Big], \qquad (A.32)$$

where

$$E_1 = \frac{b^2\gamma}{N^2C_2^2},$$

$$H = \frac{-\bar{Q}^*E_1}{F^2-s^2},$$

$$E_2 = \Big(\frac{1}{q}(\frac{F}{s})^3 - (1+\frac{1}{q})(\frac{F}{s})\Big) H +$$

$$+ E_1\Big(\frac{1}{q}(\frac{F}{s})^2-1\Big) \frac{\bar{Q}^*}{sF},$$

$$E_3 = -N^2E_2 - (N^2-2)(\frac{F}{s})H - \frac{b^2\gamma\bar{Q}^*}{C_2^2sF},$$

$$E_4 = -E_2(\frac{F}{s}) + H,$$

$$E_5 = -(N^2-2)E_2 - N^2(\frac{F}{s})H - \frac{b^2\gamma\bar{Q}^*}{C_2^2sF},$$

$$C^* = (E_4+E_5)s/2,$$

$$A^* = (1- \frac{1}{q})(\frac{1}{s})C^* - \frac{E_4}{2},$$

References

1. Kennedy, F. E., and Karpe, S. A., "Thermo-cracking of a Mechanical Face Seal," Wear, 79 (1982) pp.21-36.

2. Burton, R. A., "Thermo-mechanical Effects in Sliding Wear," Workshop on Frictionally Induced Thermal Deformation and Wear, Annapolis, MD, June 19-20, 1979.

3. Sibley, L. B., and Allen, C. M., ASME Paper 61-Lub-1S, 1961.

4. Ling, F. F., and Mow, V. C., "Surface Displacement of a Convective Elastic Half-Space Under an Arbitrarily Distributed Fast-Moving Heat Source," J. Basic Eng. September 1965, pp.729-734.

5. Mow, V. C., and Cheng, H. S., "Thermal Stresses in an Elastic Half-Space Associated with an Arbitrarily Distributed Moving Heat Source," Z. Angrew. Math. Phys., 18, (1967), pp.500-507.

6. Ling, F. F., and Yang, C. C., "Temperature Distribution in a Semi-Infinite Solid Under a Fast-Moving Arbitrarily Heat Source," Int. J. Heat Mass Transfer, 14, pp.199-206.

7. Ju, F. D., and Huang, J.H., "Heat Checking in the Contact Zone of a Bearing Seal," Wear, 79 (1982) pp.107-118.

8. Ju, F. D., and Chen, T.Y., "Thermo-mechanical Cracking in Layered Media from Moving Friction Load," J. of Tribology, Oct. 1984, pp.513-518.

9. Ju, F. D., and Huang, J. H., "Thermo-mechanical Cracking Due to Moving Friction Loads," UNM Report No. ME-125(84)ONR-233-2, May, 1984.

10. Huang, J. H., and Ju, F. D., "Thermo-mechanical Cracking Due to Moving Friction Loads Part II. A Three Dimensional Model of a Single Asperity," Wear, 102, (1985), pp.87-97.

11. Huang, J. H., "Thermo-mechanical Cracking Due to Moving Friction Loads," Ph.D. Dissertation, University of New Mexico, July, 1984.

12. Ju, F. D. and Huang, J. H.," Thermo-mechanical Cracking Due to Moving Friction Loads," Proc. Mech. Failure Prevention Group, April 1985 (in print)

13. Ju, F. D., "The Asperity and Material Parameters in Thermo-mechanical Cracking Due to Moving Friction Load," UNM Report NO. ME-136(86)ONR-233-3, Feb. 1986.

14. Blau, P. J., "The Role of Metallurgical Structure in The Integrity of Sliding Solid Contacts," Solid Contact and Lubrication, ASME, AMD-v. 39, 1980, pp.185-191.

15. Ruff, A. W., and Blau, P. J., Studies of Microscopic Aspects of Wear Processes in Metal, National Bureau of Std. NBSIR 80-2085, June, 1980.

16. Boley, B. A., and Weiner, J. H.. Theory of Thermal Stress, Wiley, 1960.

17. Duhamel, J. M. G., "Memoire sur le calcul de Actions Molecularies Developpees par les Changements de Temperature dans le corps solids." Memoires ... Par diveis savan ts, 5, 1838, pp.440-498.

18. Parkus, H., Instationare Warmeshannungen, (Russiann trans.), Springer-Verlag, Wien, 1959.

19. Danilovskaya, V. I., "Thermal Stresses in an Elastic Half-Space Arising After a Sudden Heating of Its Boundary," Prikl. Mat. Mekh., 14, May-June 1950, pp.316-318.

20. Danilovskaya, V. I., "On a Dynamical Problem of Thermo-elasticity," Prikl. Mat. Mekh., 16, No 3, May-June 1952, pp.341-344

21. Carslaw, M. S., and Jaeger, J. C., Conduction of Heat in Solids, Clarendon Press, Oxford, 1959.

22. Burton, R. A., Friction and Wear, chap. 2, Tribology, ed. A. Z. Szeri, McGraw-Hill, 1980, pp.17-38.

Forsythe, G. E., Malcolm, J. H., and Moler C. B., Computer Methods for Mathematical Computations, Prentice-Hall, Inc.

F. F., Surface Mechanics, John Wiley & Sons, Inc.

END

10-87

DTIC